Properties of Close Pairs of Galaxies

by

Henry Joy McCracken
B.Sc., University of Manchester 1991

A Thesis Submitted in Paritial Fulfillment of the
Requirements for the Degree of

MASTER OF SCIENCE

in the Department of Physics and Astronomy

We accept this thesis as conforming
to the required standard.

[redacted]

Dr. C. Pritchet, Supervisor (Department of Physics & Astronomy)

[redacted]

Dr. D. Hartwick, Departmental Member (Department of Physics & Astronomy)

[redacted]

Dr. P. Wood, Outside Member (Department of History)

[redacted]

Dr. S. Morris, External Examiner (Dominion Astrophysical Observatory)

Supervisor: Dr. C. J. Pritchet

Abstract

Colour and clustering properties of galaxies at small angular separations are investigated using three new galaxy catalogues and the following conclusions are drawn:

Firstly, field galaxies are slightly redder than paired galaxies, and the correlation amplitude of redder galaxies is found to be higher than that of bluer galaxies. These results are interpreted as a consequence of the higher correlation strength of early-type galaxies.

Secondly, the small-angle correlation function is well described by extrapolation of the (large-angle) Infante and Pritchet (1995) correlation functions to these separations. Pair count ratios in two angular bins agree well with predictions of these correlation functions. These results argue there is no excess in close pairs of galaxies, a result found for all three catalogues.

Lastly, the low small-separation correlation amplitudes found indicate that the fraction of galaxies in *physical* pairs at these separations is small. Consequently, this implies that merger detection by pair/field colour differences is difficult and would require larger sample than currently available.

The low merger rates derived for our sample, together with low correlation function amplitudes and lack of excess over the Infante and Pritchet correlation functions argue against significant merging in the galaxy population as described by scenarios like Broadhurst et al. (1988). Consequently, we prefer models in which the faint blue excess is explained in terms of starbursting dwarf galaxies or an incorrectly determined local luminosity function.

[redacted]

Dr. C. Pritchet, Supervisor (Department of Physics & Astronomy)

[redacted]

Dr. D. Hartwick, Departmental Member (Department of Physics & Astronomy)

[redacted]

Dr. P. Wood, Outside Member (Department of History)

[redacted]

Dr. S. Morris, External Examiner (Dominion Astrophysical Observatory)

Contents

List of Tables

List of Figures

Acknowledgments

I would like to thank my supervisor, Dr. C. J. Pritchet, for intellectual and financial support. Without him, my sojourn in Victoria would not have been possible, and I would have been relegated to scouring the streets of Manchester for jobs in the mills (maybe).

Thanks also go to the many friends I have made in Victoria, and to the denizens of the Fourth Floor of that masterpiece of concrete, the Elliott Building, who have made my stay here unusually enjoyable.

I'd also like to thank Tom Waits, Nick Cave, Leonard Cohen and Jim Jarmusch (for spiritual guidance), and whoever it was that discovered that beans of a certain plant when roasted, ground and put in boiling water make an amazingly good beverage.

Chapter 1

Introduction

The past quarter-century of astronomical observations has established with certainty that galaxies are *not* uniformly distributed across the sky; they are correlated. The strength of this correlation, described by the angular correlation function and discussed below, is larger at smaller separations and is found to be well approximated by a power-law.

Throughout this discussion we will encounter the term "angular correlation function" and so we will do well to define it now. This quantity, commonly represented by $\omega(\theta)$, is a measurement of the *number of galaxies at a given angular separation in excess of that expected from a purely random distribution*. Hence, $\omega(\theta)$ is a very useful statistic for measuring the amount of clustering present in a sample of galaxies. Its enduring popularity amongst observational cosmologists is due to the ease with which it may be measured– all one requires are galaxy positions and magnitudes. Unlike $\xi(r)$, the spatial correlation function galaxy, redshifts (which are commonly interpreted as distances) are not required– which is fortuitous for the observer, as a much greater amount of telescope time is required to measure an object's redshift

than its magnitude.

1.1 Surveying the Universe

One of the earliest large-scale surveys of the sky was performed at the Lick Observatory by Shane and Wirtanen (1967) and consisted of 1246 plates each of size 6° by 6°. On each plate galaxies were counted in boxes 10′ by 10′, giving 36 × 36 cells for each plate. These counts were stored on microfilm for later use.

When the Shane-Wirtanen counts were plotted by assigning intensity values proportional to the number of galaxies found in each of the cells (Seldner et al., 1977) the non-uniform nature of the distribution of bright galaxies became apparent. Furthermore, when the data were later analysed by the statistical methods which were just becoming available (Groth and Peebles, 1977) it was found that over a wide range in angle,

$$\omega(\theta) \propto \theta^{-\delta} \tag{1.1}$$

where $\delta = 0.6 - 0.7$. In addition, it was also determined that at large angular scales the amplitude of $\omega(\theta)$ dropped abruptly to zero.

With the advent of automatic scanning machines in the 1970's large amounts of plate material, primarily from Schmidt telescopes, were digitised and processed in an attempt to further understand the properties of $\omega(\theta)$. One such study is that of Shanks, Fong and Ellis (1980). They measured $\omega(\theta)$ to a limiting magnitude of $J = 21.5$ and $R = 19.75$ on five plates taken at the UK Schmidt telescope. They confirmed that the correlation function can

be described by a power law of slope ~ 0.8. Furthermore, they confirmed the "scaling" behaviour of $\omega(\theta)$; namely, the correlation amplitude A_ω decreases for fainter samples.

1.2 Counting Galaxies

In parallel with work determining $\omega(\theta)$, the same plate material was being used to determine how the observed numbers of galaxies changes as a function of apparent magnitude (Tyson and Jarvis, 1979). The studies discovered that at fainter limiting magnitudes the number of galaxies observed *exceeded* that predicted by models in which galaxy luminosity or colour does not change from earlier epochs (referred to as the "No Evolution" or NE models in the literature). γ_{obs} (the slope of the number counts-magnitude relation or $dlogN/dm$) in the b_J ($b_J \sim J$) passband is found to be 0.455 , compared with a no-evolution result γ_{NE} of 0.36. This implies a $4\times$ excess over NE models by $b_J = 24$ (Peterson et al., 1979).

In addition, it was soon well established that there is a general trend towards bluer colours for fainter galaxies. Stated another way, γ is shallower for the redder bandpasses than for bluer ones. A recent review article by Koo and Kron (1992) collates number counts taken in three bandpasses, the blue b_J (4500 Å), the red (Gunn r, 6500 Å) and the near infra-red (K, 6500 Å) bands. This is presented in Figure 1.1. From this figure it is immediately apparent that the NE models easily fit the data in the K band whilst in the r band agreement is worse and in b_J very much worse. Taken together, the combined number counts and colour information argue that there is a

large population of faint ($b_J < 22$) blue galaxies which are not apparent in present-day galaxy samples.

1.3 Faint Galaxy Redshifts

Photometry alone cannot hope to address the nature of the faint blue galaxy excess– one cannot determine whether the faint galaxies observed are *intrinsically* faint (low absolute luminosity) and therefore nearby– or whether they are instrinsically bright and far away. Only by measuring redshifts can one distinguish between these scenarios.

The redshift furnishes an important quantity. The expansion of the Universe causes distant galaxies to appear as if they are receding from us; furthermore, Hubble discovered the important result that this "velocity" of recession was proportional to a galaxy's distance from us. Consequently, if we interpret the shift of the galaxy's spectrum towards longer wavelengths (the "red-shift") as arising from expansion of space (an interpretation supported by cosmological considerations) then redshift measurements correspond to distance measurements through Hubble's constant of proportionality, H_O.

Measuring a galaxy's redshift is, however, a much more difficult matter than measuring its apparent magnitude. Traditionally, one would image the target galaxy through a dispersive element such as a grating or prism. The light from the galaxy, instead of being localised in an image, is now spread out along the dispersion axis of the instrument. Consequently, the surface brightness of the image is reduced and therefore longer integration times are required to achieve the same signal-to-noise which one would achieve

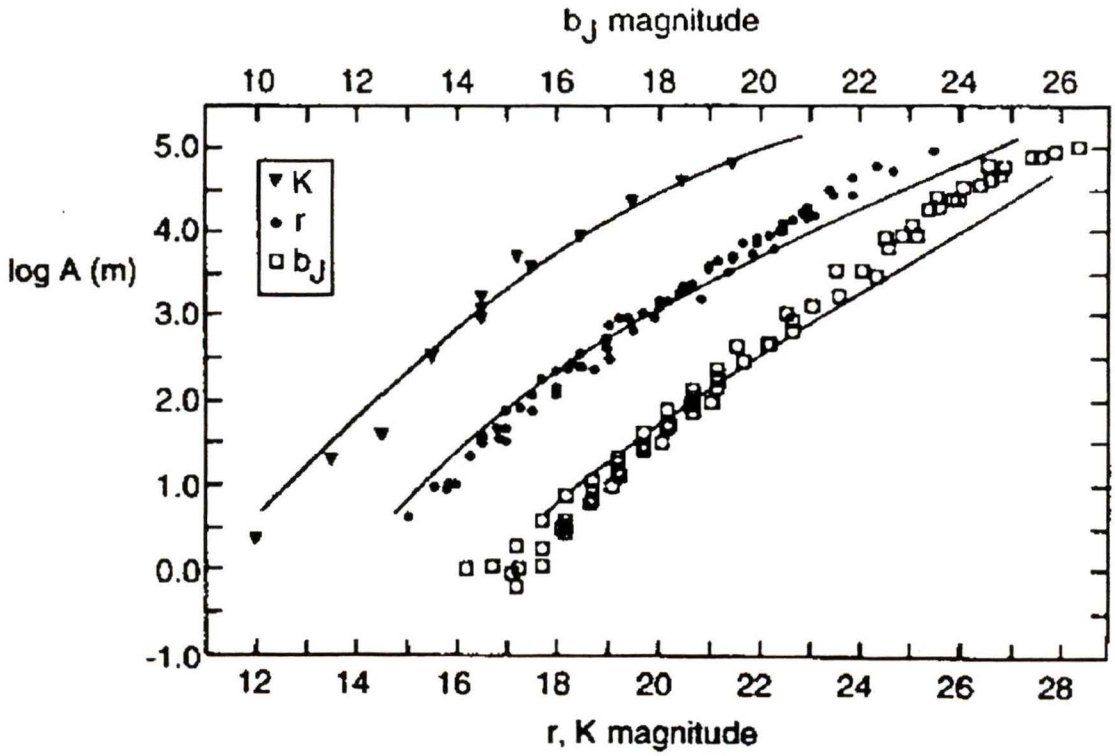

Figure 1.1: Differential Galaxy Number Counts $A(M)$ (Koo and Kron, 1992) per square degree per square magnitude in b_J (blue, 4500 Å) , r (red, 6500 Å) and K (near-infrared, 2.3 μm) bandpasses . The solid line represents Koo and Kron's no-evolution model.

in direct-imaging mode. Furthermore, the *resolution* of the spectrograph– the number of angstroms per millimeter of detector area– directly affects the required integration time. High resolution spectroscopy requires high dispersions and therefore lower surface brightnesses and longer integration times.

As if these considerations were not discouraging enough, there are cosmological factors which make the instrumentalist's task even more arduous. Galaxy surface brightnesses are strongly dependent on redshift; the photon rate per angular resolution element depends on $(1+z)^{-3}$; if we assume that rest frame flux can be approximated by $f_\nu \sim \nu^{-2}$ then the signal to noise is given by $(1+z)^{-5}$ and the time required to achieve a given signal-to-noise is $(1+z)^{10}$ (Koo and Kron, 1992)!

Despite these unpleasant facts two developments have made the measurement of large numbers of redshifts of "normal" galaxies (i.e., ones whose luminosity L is similar to the Milky Way, L^*) at a significant redshifts (by this we mean $z > 0.1$, or look-back times corresponding to one-tenth the Hubble age of the Universe) a possibility. Firstly, the development of CCD detectors whose quantum efficiency (QE)– a measurement of how sensitive the detector is to incident radiation– is many times greater than that of photographic emulsions. Photographic plates typically have a QE of a few percent, whilst today CCD cameras with QE of 50% or more are not uncommon. Secondly, multi-object spectrographs allow one to collect many redshifts at once. One such instrument is the Anglo-Australian Telescope 2-degree field Fiber Spectrograph (AAT 2df FS). This instrument uses fiber optic cables to collect light from 400 sources and feed them to a spectrograph and CCD camera.

One of the earliest studies which attempted to identify the faint blue count excess in spectroscopic surveys was that of Broadhurst, Ellis and Shanks (1988). Their survey attained a depth of $b_J = 21.5$ (note that this survey, and others like it, are all limited in *magnitude* and not redshift). They discovered, remarkably, that the galaxy redshift distribution $N(z)$ was well matched by predictions of the NE models. The counts excess at this limiting magnitude is small ($\sim 30\%$) but subsequent surveys (Colless et al., 1990), (Colless et al., 1990) to greater limiting depths have confirmed there is no evidence of deviation from NE models to $b_J < 24$. In addition, they examined the equivalent widths W_λ of the OII line (thought to be a strong indicator of star formation) and found that objects with *strong* OII ($W_\lambda > 20$Å) had $\gamma = 0.61$ whilst objects with weaker OII ($W_\lambda < 20$ Å) had $\gamma = 0.28$ indicating that the strong-lined OII sources are making a contribution to steepening the number counts.

To account for their results they proposed that that the steep slope of the number counts could be explained by low luminosity galaxies undergoing bursts of star formation. They also argued that models including evolution of a significant fraction of field galaxies were ruled out by the redshift distribution.

Many more surveys have been conducted since their work (Colless et al., 1993), to increasing degrees of completeness. These surveys confirm that the redshift distribution is matched by no-evolution predictions and furthermore that no evidence exists for a high or low tail to the distribution. Most surprisingly, the median redshifts of the surveys are remarkably low; for example, (Colless et al., 1993) found *no* galaxies with $z > 0.7$. The redshift

distribution determined by Colless et al. (1993) to a limiting magnitude of $B = 22.5$ is illustrated in Figure 1.2.

1.4 Recent Determinations of $\omega(\theta)$

The Schmidt plate surveys outlined in Section 1.1 soon progressed to prime focus plates taken at 4-metre class telescopes. These surveys had two important advantages over earlier works: firstly, the plate scale was much larger, permitting better angular resolution and resulting in improved star/galaxy separation; secondly, the larger telescope apertures allowed $\omega(\theta)$ to be determined to depths at which galaxy evolution might be expected to play a significant role in determining its shape. The redshift distribution of galaxies, seen in projection on the sky as the overlapping of many galaxies, will affect the value of $\omega(\theta)$ found at progressively fainter and fainter limiting magnitudes.

1.5 Probing Galaxy Evolution with $\omega(\theta)$

Theoretical determinations of $\omega(\theta)$ have been presented in many places (Infante and Pritchet, 1995; Cole et al., 1994b; Brainerd et al., 1994; Roche et al., 1993); these discussions are useful to us because they help us to understand what factors influence the observed angular correlation. Briefly, $\omega(\theta)$ is calculated from $\xi(r)$, the spatial correlation function, by *Limber's Equation*. $\xi(r)$ expresses the *three-dimensional* correlation of galaxies; it tells us how many objects there are within a radius r in excess of random. We may express $\xi(r)$ as

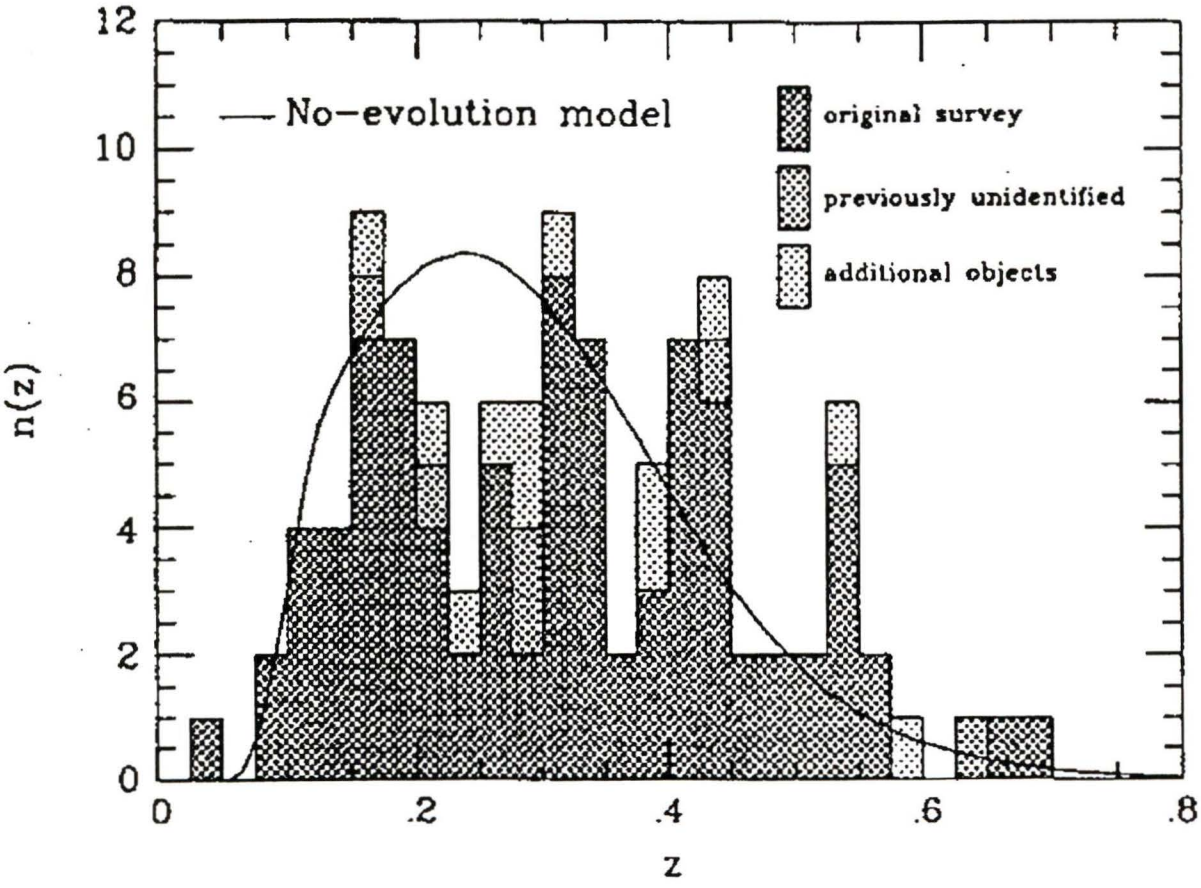

Figure 1.2: The redshift distribution for a sample of faint galaxies (Colless et al., 1993) to a limiting magnitude of $B = 22.5$. The solid line indicates the predictions of a No-Evolution galaxy model.

$$\xi(r,z) = (r_0/r)^{\gamma}(1+z)^{-(3+\epsilon)} \tag{1.2}$$

This equation contains several important parameters. Firstly, r_0 is known as the *correlation length*. Redshift surveys (references) have measured r_0 and γ; typically $r_0 = 5.5h^{-1}$ Mpc and $\gamma = 1.8$. ϵ describes how $\xi(r)$ evolves as a function of redshift. Traditionally, it is assumed that $-1.2 < \epsilon < 0$, which corresponds either to clustering fixed in proper co-ordinates ($\epsilon = 0$) or, to clustering fixed in co-moving co-ordinates ($\epsilon = -1.2$). Choosing the correct value for ϵ is difficult. One may attempt to model galaxy evolution numerically (typically by N-body simulations on supercomputers) and use this to deduce what value of ϵ produces the observed galaxy distribution. Rapid clustering evolution (i.e., $\epsilon > 0$) is largely ruled out by the low median redshift of the faint field galaxy population. One may note in passing that there is *no* dependency on H_0, the Hubble Constant, in the correlation amplitude calculations.

Evaluation of Limber's Equation requires that $\xi(r)$ is integrated over redshift space. To accomplish this we must supply an additional quantity, the redshift distribution of galaxies $N(z)$; a recent determination of $N(z)$ has already been presented in Figure 1.2.

The "scaling" of $\omega(\theta)$ describes how the correlation amplitude at a certain separation (in this work 1′) varies as a function of the sample's limiting magnitude. We may use the procedure outlined above to calculate A_ω at successively fainter ($J < 21$) magnitudes. These predicted A_ω's are found to be *much higher* than those observed (Roche et al., 1993; Brainerd et al.,

1994; Pritchet and Infante, 1992a; Koo and Szalay, 1984; Bernstein et al., 1994). (The calculations are performed using a "standard model", i.e., one which does not incorporate luminosity evolution). In other words, the faint galaxy population is much more weakly clustered (by about $\times 4$ or $\times 5$ at $J \sim 24$) than the predictions of the no-evolution models.

In an early investigation (Koo and Szalay, 1984) the evolution of $\omega(\theta)$was determined to a limiting magnitude of $J \sim 24$. From their survey they determined the scaling of $\omega(\theta)$ and were able to conclude that galaxies had undergone "some, but mild" luminosity evolution. They did this by comparing their observations to models of galaxy evolution which predicted the shallower slope at fainter magnitudes which they observed in their sample.

Following on from their earlier work in the South Galactic Pole, Pritchet and Infante measured $\omega(\theta)$ in five adjacent fields at the North Galactic Pole (NGP) in two bandpasses, J and F to a limiting magnitude of $J \sim 24$ (Pritchet and Infante, 1992a; Pritchet and Infante, 1992b). Their data had wide angular coverage (> 2.2 deg^2) and good resolution (FWHM $< 1''$ on all frames); in addition they measured the zero point and scale variations across their plates. They were able to confirm (i) that the amplitude of A_ω decreased with increasing limiting magnitude and (ii) The slope of the correlation function, δ also decreased with increasing limiting magnitude.

CCD detectors have permitted investigations of the scaling behaviour of $\omega(\theta)$ to fainter magnitudes. However, these studies were initially plagued by the smaller field of view of CCDs which resulted in much smaller numbers of galaxies in the survey, which is unfortunate as errors in the correlation function measurement in each angular bin are approximately Poissonian –

i.e., they scale as $1/\sqrt{N}$, where N is the number of galaxies in each bin.

A number of objects are known to have smaller correlation lengths than the canonical $5.5h^{-1}$Mpc. For example, galaxies observed by the IRAS satellite are known to have a correlation length of $r_0 = 3.8h^{-1}$Mpc. It is possible that a type-dependent measurement of the correlation function would show that the correlation amplitude does not change with time; our current measurements of the low correlation amplitude of faint galaxies would then be interpreted as indicating merely a different morphological mix at past epochs.

This result, taken with the count excess problem outlined previously, suggests that the excess population identified in the number counts is also *weakly clustered*. This result at first appears to present problems for us, because we seek to explain the decline in number density from $z \sim 0.3$ to the present day by postulating merging in the galaxy population. However, we must consider that at $z \sim 0.3$ the mean density of galaxies is much higher because the universe is much smaller. In fact, the number density of galaxies as a function of z has roughly the form $(1 + z)^2$ per unit redshift. Furthermore, dwarf galaxies which are thought to comprise the starbusting population have a much higher number density than L^* galaxies (Infante and Pritchet, 1995).

We may summarise the main conclusions drawn from recent work on the scaling behaviour of $\omega(\theta)$ as follows.

- Observational data (redshift distribution, correlation lengths and slope) and one theoretical parameter (growth of clustering) predict an amplitude of A_ω which is a factor of 2-3 higher than that observed.

- To explain the low observed value of A_w it is proposed that a weakly clustered population dilutes its strength.

- Considerable evidence already exists that different galaxy types have different correlation lengths. If the morphological mix of galaxies were different at $z = 0.3$ then this could explain the observations.

1.6 Why Study $\omega(\theta)$ at Small Separations?

We are now in a position to understand the motivation of our work. We have discussed how information gleaned from the shape and form of $\omega(\theta)$at large angular separations can reveal details concerning the macroscopic nature of the Universe. But there is also useful information in the *small scale* behaviour of $\omega(\theta)$.

It has been suggested (Broadhurst et al., 1992) that the merging of galaxies could explain the excess in the number counts at intermediate redshifts, sometimes referred to as *number evolution* in the literature. In this scenario, galaxy mergers reduce the number counts to their observed value. In addition, the merger event is thought to trigger a burst of star formation and therefore be responsible for the strong OII lines and bluer colours characteristic of the excess population.

As we have already discussed, measurement of $\omega(\theta)$ is quite sensitive to changes in the galaxy population as a function of look-back time. In the previous section we discussed the variation of the correlation amplitude as a function of the sample's limiting magnitude. Comparing these variations to theoretical predictions tells us that the overall galaxy population at $z \sim$

0.3 was much more weakly clustered than the contemporary one. However, there is another property of the correlation function we can investigate as a means of learning more concerning galaxy populations– namely, how, *for a given magnitude range*, the amplitude of the correlation function varies as a function of angular separation.

As we have already described, many investigators have found that the correlation function is well described by a power law at intermediate separations, i.e., in log-log plots a straight line fits the data well. However, at large angles ($\log(\theta) > -1$, where θ is measured in degrees), some workers have detected the presence of a "break" in the correlation function (Infante and Pritchet, 1995), i.e., correlation power drops abruptly to zero. Conversely, at smaller angles ($\log(\theta) < -3$) at least one study (Carlberg et al., 1994) has suggested that there may be an "excess" in the correlation function; that is, that the amplitude of the correlation function is significantly higher ($> 2 - 6\times$) than predicted by a power law fit at larger separations.

Such deviation from power-law behaviour could have important implications for theories which attempt to explain the number count excess and the lower correlation amplitude problems outlined above. If the median redshift of our sample is ~ 0.3 then angular separations of $\theta \sim 6''$ correspond to physical separations of $\sim 20h^{-1}$ kpc. If galaxies separated by this amount were to interact then the classical pictures of galaxy evolution (Larson and Tinsley, 1978) suggests that such interactions trigger star formation which in turn causes a blueing of the galaxy colours. Models exist in which the blue number count excess in galaxy populations is explained by some fraction of the galaxy population undergoing merging events such as the ones

outlined above. These models also predict the *number* of galaxies which are undergoing such merging events.

Measurement of the correlation function at small separations can tell us how many galaxies are separated by small amounts (after projection effects are allowed for); comparing the numbers found from such studies with those needed for a viable merging scenario is an important test of any merger model.

1.7 This Study

This current work is based on plate material which has already been described and analysed (Pritchet and Infante, 1992a; Pritchet and Infante, 1992b; Infante and Pritchet, 1995). In these papers the authors were primarily interested in the behaviour of $\omega(\theta)$ at *large* separations, and consequently their analysis was considerably different from the current one. At large separations, $\omega(\theta)$ is very small and therefore more prone to errors and biases. In the current work we are interested in the behaviour of $\omega(\theta)$ at small separations, and consequently we do not need to carry out many of the steps which a larger-angle study would merit.

More importantly, doubts exist concerning the reliability of the Pritchet & Infante results at the small separations which we consider ($1'' < \theta < 6''$). For example, the Pritchet and Infante (1995) correlation functions exhibit large scatter at $\log(\theta) \sim -3$, an effect which is easily explicable in terms of misclassification or non-detection of objects (conversely, the errors which arise at larger separations are due to the edge or biasing effects outlined

above, which are must more difficult to correct for). Furthermore, object detection and finding for the Pritchet and Infante catalogues was carried out on-line on the APM plate scanner, using software at the plate scanner which was primarily written for the analysis of *stellar* data.

Conversely, in this study, raster scans of the central regions of the plates were converted to computer-readable format and reduced using software written specifically for the analysis of faint field galaxies and which has undergone extensive testing for this application (Infante, 1987). Furthermore, all objects that contribute towards the correlation function at small separations were manually inspected– quite an important precaution as large numbers of these objects are spurious. Failure to remove such objects would lead to spuriously large correlation amplitudes at small angles. All three catalogues, (J band, F band and the merged catalogue) were edited.

In this Thesis the correlation functions computed from the data sets described previously are presented.

The reliability of the $\omega(\theta)$ determined from both is dependent upon the accuracy with which spurious objects can be detected and rejected. However, there are fewer objects in the matched catalogues than in the unmatched catalogues, which consequently means that the statistical noise in these correlation functions will be larger. In addition, plots of colour, magnitude, and magnitude difference of paired objects in the samples are also presented.

Chapter 2

Reducing the Data

2.1 Characteristics of the Plates

Nine plates of the north galactic pole (NGP) were taken at the CFHT in May 1987. This direction points out of the plane of our galaxy and hence contamination of the frames by foreground stars belonging to the Milky Way is minimised. Furthermore, the areas examine are arranged in a "chequerboard" pattern on the sky which minimises the noise in the angular correlation function. At the faintest magnitudes considered in the survey, J $\sim$ 23, only 10% of the objects visible are stars.

Each photographic plate covers an area of 0.84 deg^2 and has a plate scale of 13.64"mm^{-1}. Seeing (expressed as the full-width at half maximum of a gaussian profile) was $< 1''$ for all frames. The emulsions and filter combinations used were IIIaJ+GG385 (J - band) and IIIaF + GG495 (F-band), chosen to closely match passbands of previous workers. The response of IIIaJ filter/emulsion combination drops steeply at $\sim$ 5500Å, whilst IIIaF combination drops at longer wavelengths, $\sim$ 7000 Å, making the former more

sensitive to bluer objects, and the latter better suited for studying redder objects. The notation we will use to describe the plates consists of a number (indicating the field number) and a letter (indicating the bandpass, either J or F). Field numbers range from $1-5$ for J and $3-5$ for F. Field $2F$ was not available due to scanning errors (different part of the scanned field were not in alignment with each other), whilst poor weather prevented taking field $1F$.

2.2 The Plate Measuring Machine

The data was scanned with the Automatic Plate Measuring Machine (APM) in two modes. For the first mode– the *image* mode– the entire plate was scanned at steps of 16μm and on-line software was used to construct parameters for each object on the plate with area and brightness above some pre-specified limit. This object data was written to tape as scanning proceeded.

The second APM mode– known as the *raster* mode– differs radically from the image mode in that no detection or measurement of objects is carried out. Rather, an image of the central 0.22 deg^2

of each photographic plate (this region was arbitrary chosen to exclude "bad" areas of the plate) is written to tape. For this mode the slightly larger scanning interval of 31 μm is used. This corresponds to a pixel scale of $0.423''$ in the digitised frame. Each of the final FITS images occupies approximately 32 megabytes of disk space if 16 bit numbers are used (which is justified given the poor dynamic range of photographic density).

The CFHT NGP survey, described in Pritchet and Infante (1992a), used the image-mode data and not the raster scans. This approach has the advantage of requiring much less processing time than using the raw frame data would. This was an important consideration when the data was taken but is not today given the increase in available computing power.

The main objection to using image-mode data concerns the ability of the APM software to separate closely spaced objects, which has been called into question by several workers ((Carlberg et al., 1994), (Pritchet and Infante, 1992a)) . For this reason, we prefer to use our own software to perform object detection and photometry on the raster scans and furthermore to verify that such detections are correct by visually inspecting *all* closely-separated objects.

2.3 Linearising the Scans

It is an unfortunate fact of astronomical life that photographic emulsions do not respond linearly to light falling on them. Stated another way, the amount of plate blackening (density) is *not* proportional to the incident light. In order to accurately measure the intensity of faint objects we must therefore find some way of converting non-linear photographic *densities* to linear *intensity* measurements.

Many schemes have been proposed to deal with the non-linearity of photographic plates. One (obvious) approach is to illuminate small regions of the plate with a carefully calibrated light source. If many such exposures are made then one may plot the (known) intensity of the light source against the

density recorded with the plate measuring machine. This calibration curve then may be used to convert the plate density to intensity.

This scheme has several drawbacks, not the least of which is the need to make the "sensitometer spots" in the first place! In addition, using an isolated segment (usually the corner or the edge is used) of the plate to calculate the density-to-intensity transformation for the entire plate is not a good idea as there can be significant variations in sensitivity between the peripheral regions where the spots are recorded and the useful area of the plate. In addition, although sensitometer spots were recorded on the plates for the CFHT NGP survey, these were outside the region scanned.

To linearise our plates we used an alternate approach which uses the *entire* frame to construct the density-to-intensity relation. This method makes use of the fact that, since stars are point sources, the shape of a star's intensity profile is the same regardless of its brightness. If we use all the available stars on our frames we can derive a calibration which is valid over the entire range of brightness of stellar images on the plate, between the plate limit and the brightest stars in the field.

The method we use (Bunclarke and Irwin, 1992) is implemented in APM reduction software made available by Polo Infante. The scheme proceeds as follows:

- First the raster scans are analysed with the APM "images" program. This program simulates the APM image mode and produces a set of parameters for each object in the frame. The parameters that we are most interested in are the eight *areal profiles*. These areal profiles

measure the area of the object at each of eight fixed levels of density, measured relative to the detection threshold.

- Next, these image parameters are used to determine which objects on the frames are stars and which are not. (The problem of star/galaxy separation is dealt with more fully later in section 2.8.)

- We now make the assumption that the area profiles closest to the sky values are linearly related to plate density. We use this guess to construct an initial stellar intensity profile which will then be improved iteratively.

- Next the stars are sorted by magnitude into many bins and the luminosities of stars in each bin are computed using the "first guess" standard profile and calibration information. These luminosities are used to recompute the calibration curve and then the standard profile is recomputed using calibration and luminosity information.

- The iterative technique outlined above is repeated until no further change occurs in the model profile.

- Finally, the calibration curve derived above is applied to the image.

This entire procedure is repeated until the calibration curve derived from the image does not change.

A more detailed description of this procedure can be found in Pritchet and Infante (1992b).

2.4 Finding Objects

The program we use to locate objects is called `findcyl`, kindly supplied by C. J. Pritchet. This program proceeds by a two stage process. First, the image under investigation is convolved with a Gaussian profile. Secondly, the convolved image is searched for pixels whose values are above the background by some predetermined value. An *object* is defined as a number of connected pixels (i.e., the minimum area of an object) which have this property. This detection phase is repeated a second time to separate merged objects or to combine detections which are less than one FWHM apart (the image FWHM is input into the detection algorithm).

The "convolution" process proceeds as follows. First a "kernel" is constructed from a Gaussian profile (the Gaussian profile is chosen because it closely resembles the light profile of a discrete source). This kernel array is then *convolved* with a much larger array containing the intensity values for all the pixels in the image, producing a second, *convolved* image. Each pixel in the convolved image is produced by adding the product of all the pixels around the input pixel and their corresponding pixels in the kernel array centred on that pixel.

The convolution operation acts as a low pass filter. Rapidly varying features like noise are suppressed, whilst more slowly-varying image features such as stars and galaxies are unaffected. This is illustrated in Figures 2.1 and 2.2 which demonstrate the the effect of convolution. Two features are apparent; firstly, rapidly varying noise features have been suppressed, making more slowly varying ones apparent. Secondly, the sky background has been

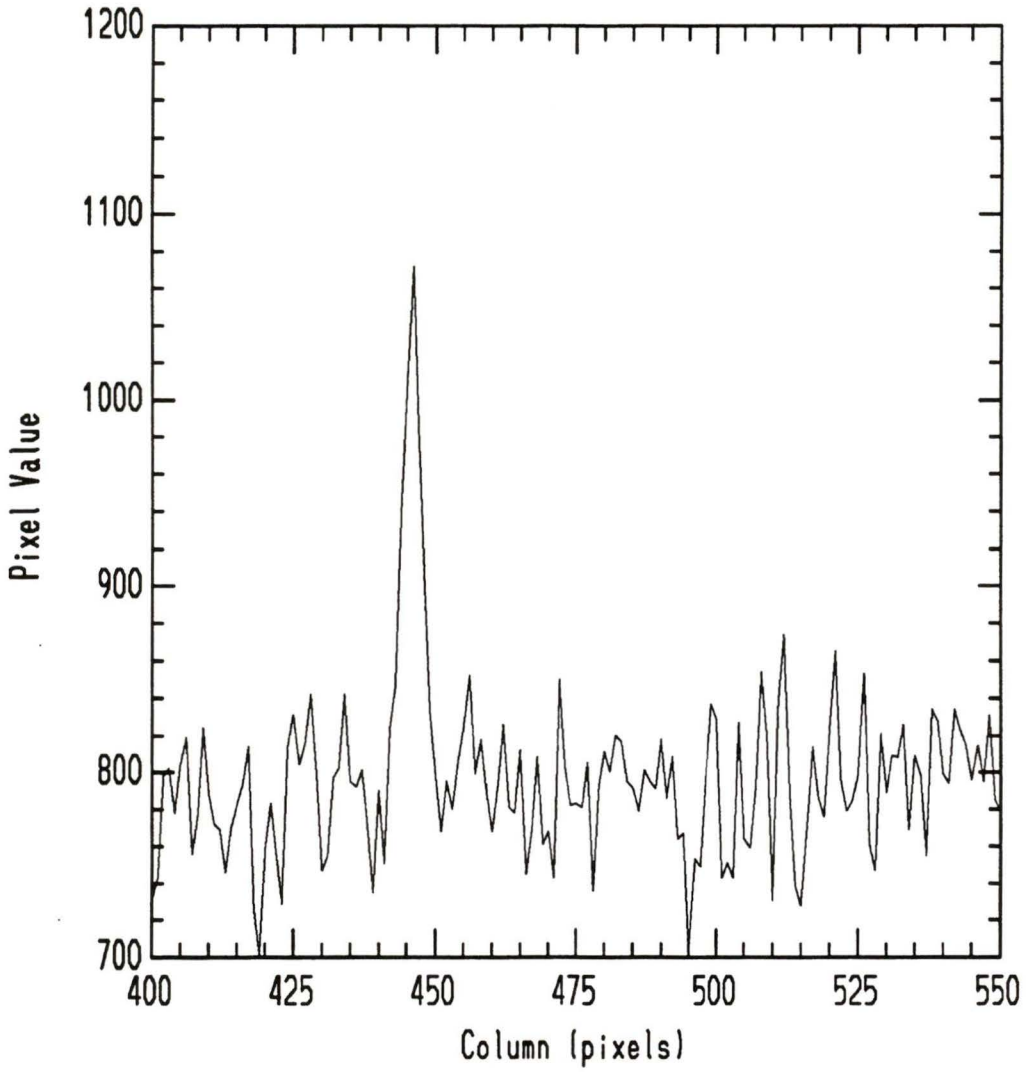

Figure 2.1: Line plot showing a row of pixel intensities from the 1J frame before the convolution process.

removed (in the low pass filter analogy, this corresponds to the signal's DC component). This is useful because in our data the sky value varies significantly across the image, which can make more simplistic detection schemes fail. Lastly, the signal-to-noise ratio has been increased. Consider the feature evident on the line plots at column 450. In the unconvolved image, this feature has a peak at around 100 units above the sky background of 850. In the convolved image, the peak is around 25 units above a sky background of 10. So in the first case the signal-to-noise ratio (S/N) is 1.2 (by inspection); similarly, in the second it is 2.50, a significant improvement.

Table 2.1 indicates a sample choice of parameters for `findcyl`. These parameters were chosen as a optimal balance between speed and accuracy (a larger convolution kernel produces a greater improvement in S/N but takes correspondingly longer to compute).

Findcyl Parameters		
Parameter	Value	Prompt
image	"apm4f2l"	Name of input image?
ocord	"apm4f2l.xy30"	name of output co-ord file?
fwhm	3.5	fwhm of input image?
nkern	9	kernel size?
thresh	30.	threshold in convlved image?
lobad	400.	minimum unsaturated data value?
hibad	8000.	maximum unsaturated data value?
redo	"y"	redo convolved image (if it exists) (y/n)

Table 2.1: Sample parameters used in program `findcyl`.

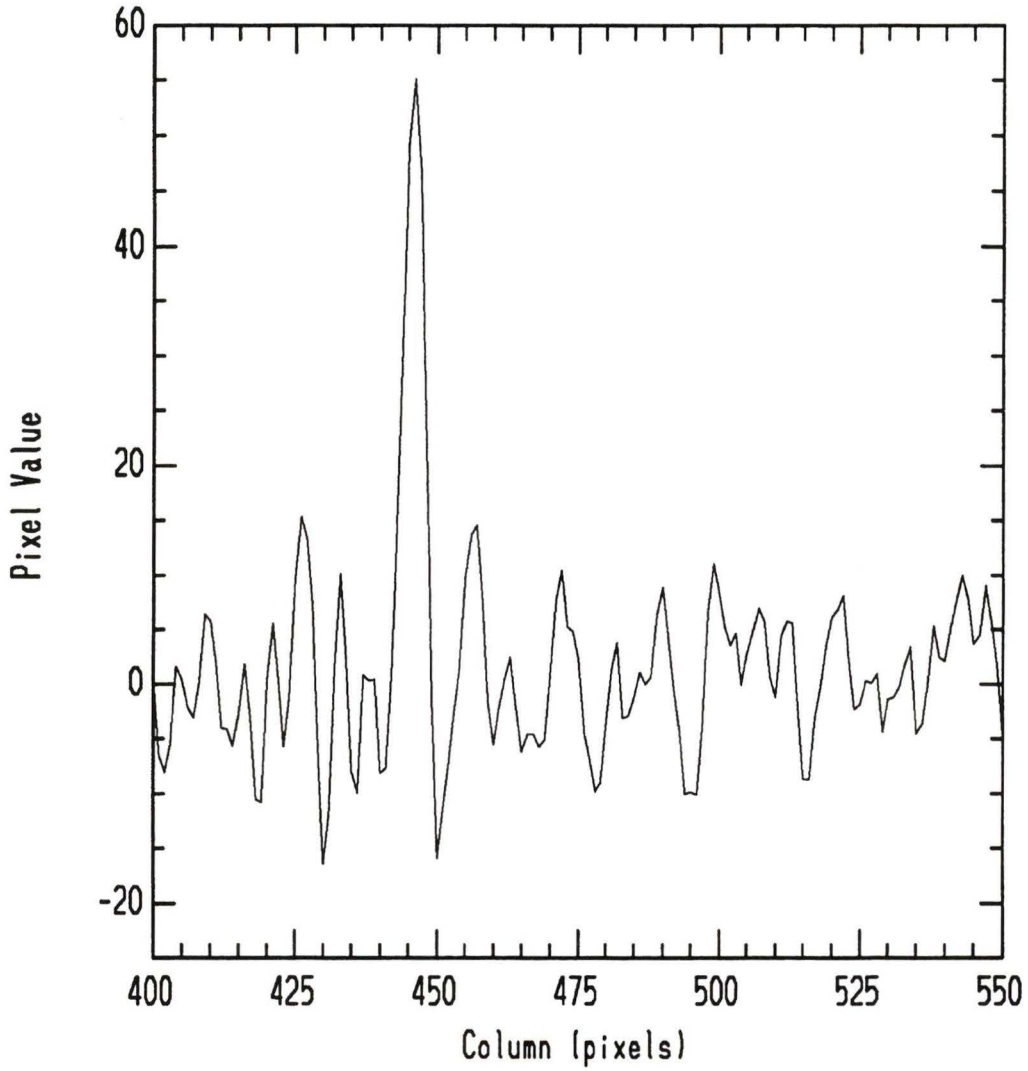

Figure 2.2: Line plot showing a row of pixel intensities after the convolution process

2.5 Photometry

Accurately measuring the flux from faint irregularly shaped objects such as galaxies is a difficult matter. One might simply measure all the counts from the target object within a fixed radius from its centre (known as *fixed aperture photometry*); this is moderately successful for stars in uncrowded fields, and is also a practical way to measure colours.

However, for unresolved diffuse objects like galaxies, this scheme has several severe drawbacks. Firstly, galaxy profiles differ vastly from object to object. Some are small in extent, with all the light concentrated near the centre, whilst others are diffuse and extended with significant amounts of light still present in the profile out to many times the FWHM of a stellar image. A large aperture, whilst including all the light from the object, has the drawback that a large amount of light from the sky is included. To accurately measure the object's magnitude, this sky value must be subtracted; and with large amounts of sky resulting from a larger aperture there must be correspondingly larger errors in the sky estimate. (Sky counts follow Poisson statistics, meaning the error goes as $\sqrt{N}$, where N is the number of pixels in the aperture. Since $N \propto r^2$, sky errors increase linearly with aperture radius). In addition, the amount of light included in the tail of the galaxy light distribution is small, resulting in poor signal to noise. On the other hand, a small aperture does not include all the flux from the object, again producing a low signal-to-noise.

From these arguments, it is apparent that there is some ideal radius which *maximises* the light included from the object but *minimises* the light

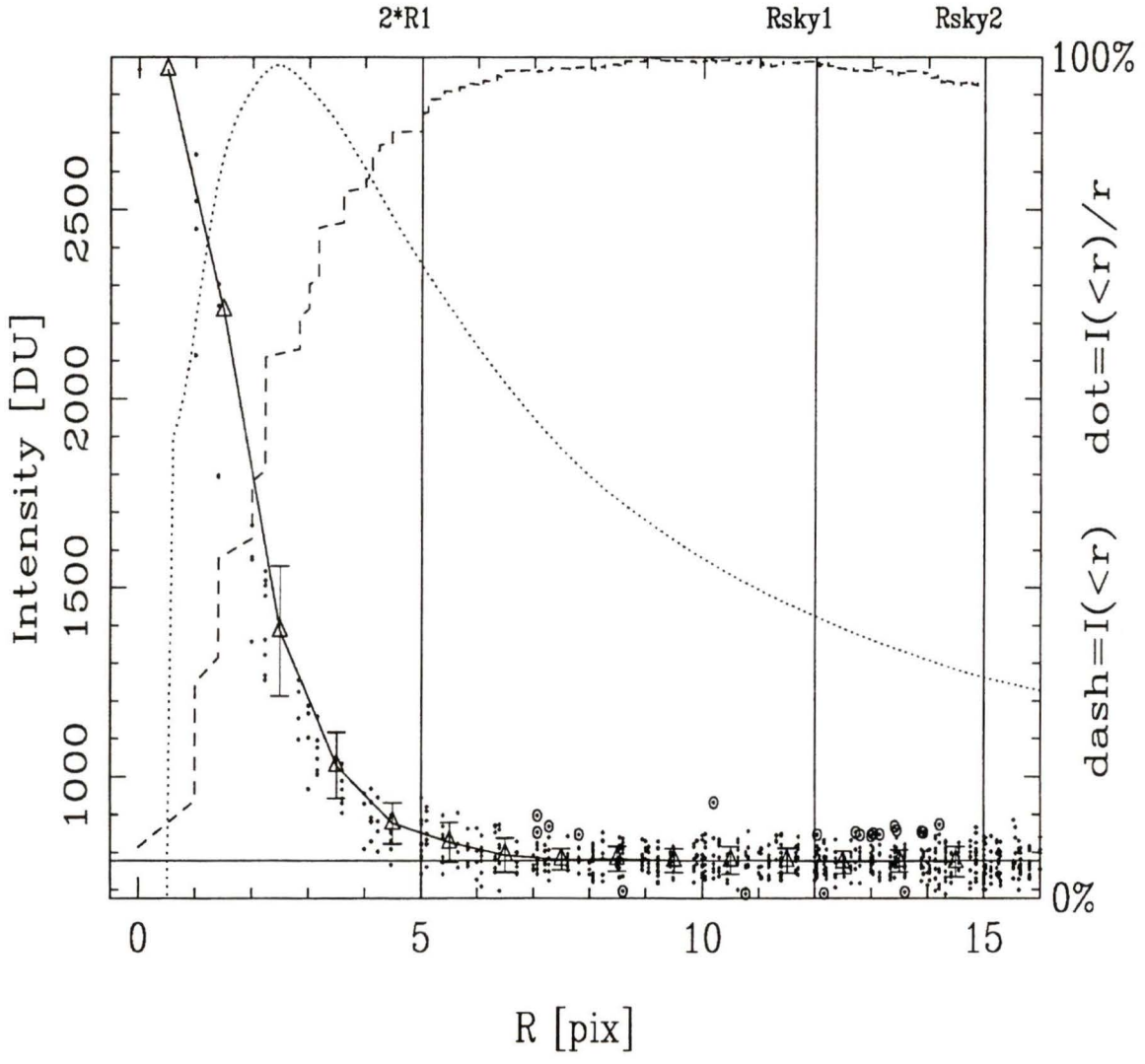

Figure 2.3: Light profile of object produced by **photkron**. The solid line indicates the mean value of the object's light profile at each of the radial bins. The dashed line represents the *curve of growth*, explained in the text. The dotted line represents $I(< r)/r$, where $I(r)$ is the object's light profile . The points represent the intensity of light in different pixels around the object. The points which are circled are those excised from the calculation.

included from the sky. Furthermore, this aperture will be different for objects of different apparent magnitudes.

The photometry program we used, **photkron**, is based on the algorithms of Kron (Kron, 1980), which address these problems. First suppose we have a galaxy whose radial profile is given by $g(r)$, where r is the distance from the galaxy's centre (whose position was determined previously by `findcyl`. Two *moments* of this radial profile are defined as follows:

$$r_1 = \frac{\int_0^\infty r g(r) dr}{\int_0^\infty g(r) dr} \tag{2.1}$$

and

$$\left(\frac{1}{r_{-2}}\right)^2 = \frac{\int_0^\infty \frac{1}{r^2} g(r) dr}{\int_0^\infty g(r)} \tag{2.2}$$

In practice, of course, the upper limit of integration is not infinity; it is normally set to be the point at which the profile intensity falls to within some predetermined fraction of the sky value. These "characteristic radii" are intensity weighted and do not depend on the sky background or signal-to-noise ratio of the image. Once r_1 is calculated then aperture photometry is performed within $2r_1$; this the value which Kron suggests gives the maximum possible signal-to-noise with the minimum amount of missed light.

To make an estimate of the sky a second aperture is chosen at some fixed distance from the object centroid (nominally chosen to be 15 pixels), and the sky value is computed from the mode of the sky values within an annulus three pixels wide at this distance.

The inverse second moment, r_{-2} measures the degree of central concentration of light in the object (by virtue of the $\frac{1}{r^2}$ weighting given to the profile intensity). This statistic is useful in distinguishing between stellar

(which are point sources and consequently have a high degree of central concentration) and non-stellar objects (which do not). In Section 2.8 we will use it to perform this task.

These ideas are illustrated in Figure 2.3 which are plots from **photkron**. The solid line with the error bars represents the mean of the light distribution for each of the radial bins. The point 2*R1, the radius at which the profile integration is halted, is also marked. The inner and outer sky annuli used are marked as Rsky1 and Rsky2. In addition, the object's *curve of growth* (dashed line) is marked. This represents the integrated light from the star within each of the radial bins.

The parameters used in **photkron** are summarised in Table 2.2.

Photkron Parameters		
Parameter	Value	Description
NANNULUS	12	number of annuli to extract
WIDTHANU	1.0	width of annuli
SKYRAD1	12.0	inner sky radius
SKYRAD2	15.0	outer sky radius
IRUPDEC	5	photometry technique
SKYFRAC	0.010	sky fraction used to calculate r_1
EXCISION	y	excise bad pixels?
REXCMIN	2.0	minimum radius for excision
ITOLFNT	2	default radius to use
RADFNT	1.0	if inner radii are less than sky
DEBUG	n	debug mode?

Table 2.2: Photkron Parameters. All values are in pixels unless otherwise noted.

2.6 Determining the Zero-Points

The linearisation process outlined above produces an *internally* consistent magnitude scale for our plates. We now have instrumental magnitudes for all the objects on our frames. (To distinguish instrumental magnitudes from true magnitudes they will be denoted by lower-case rather than upper case letters.) However, this magnitude scale still has to be tied to an *external* magnitude scale. A constant (known as the "zero point") must be added to our instrumental magnitudes to bring them into accordance with other magnitude scales. Because our calibration curve is linear over a wide range in magnitudes, we may safely use bright objects to determine the zero points for fainter objects such as galaxies.

The data that are used to calibrate our work are the catalogue files produced by PI and CJP. These are the binary files which were produced by the APM plate scanner in "images" mode. These binary files are processed by the program **catngp** which applies astrometric and photometric corrections to the raw data, producing accurate positions and magnitudes for all the objects on each of the plates. While this data may not be adequate for investigation of the small separation behaviour of $\omega(\theta)$, it is well suited to the purpose of determining the zero point of our magnitude scale.

The APM data (which will call the catngp data) was calibrated by standard stars external to the fields. It is this external calibration that the accuracy of the magnitude scale we adopt must ultimately rely upon. However, given the good agreement between galaxy number counts determined with the catngp data and previously published counts (Pritchet and Infante,

1992a), we are confident that the catngp zero-points are correct.

Before these sets of data may be intercompared, however, they must first be transformed to a common reference frame, as the scale and orientation of each is different. To accomplish this, we use a ten-term polynomial transformation kindly supplied by C. Pritchet. The transformation was determined first identifying common objects in both co-ordinate systems to determine a first-order transformation. This first order transformation was then used in conjunction with a non-linear least-squares fitting routine to determine higher-order terms in the transformation.

2.6.1 Zero Points from the Catngp Data

Calibration of raster scans proceeded as follows. First, objects on the scans were matched with objects output by catngp. For each object, the difference between the catngp magnitudes and the photkron instrumental magnitudes corresponds to the zero point of our magnitude scale. The zero point is taken to be the median value of this difference.

To check the zero-point determinations, catngp magnitudes are plotted against photkron magnitudes. This is shown in Figures 2.4 and 2.5.

This procedure was repeated for the remaining frames.

2.6.2 Checking the Data With Number Counts

Comparison of number counts determined from these catalogues with those derived from the catngp data provides us with an important test. Number counts measure the *number of objects in a given area and in a given magnitude range*. Therefore, they test both the zero-points used and the finding

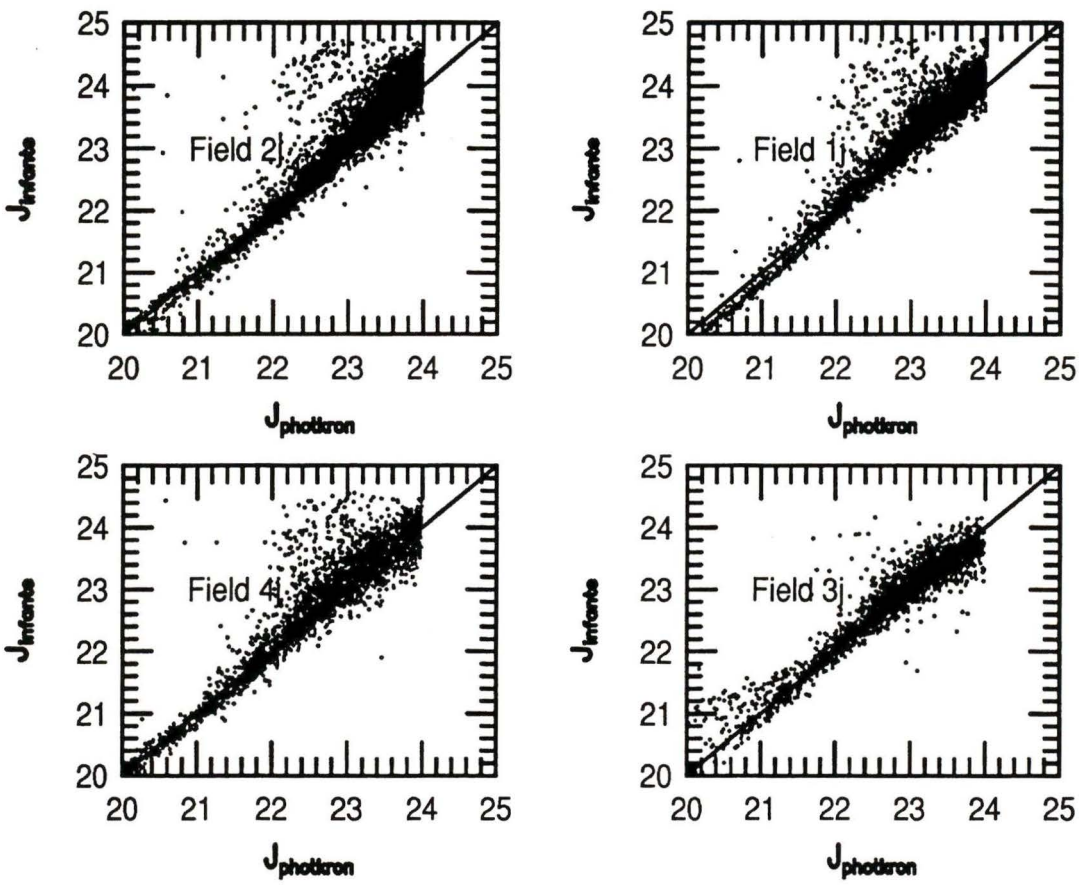

Figure 2.4: Photkron magnitudes (with zero-point added), $J_{photkron}$, plotted against catngp magnitudes, $J_{infante}$, for fields $1J$-$4J$. The solid line has a gradient of 1. The photkron catalogue includes objects in the magnitude range $20 < J < 24$.

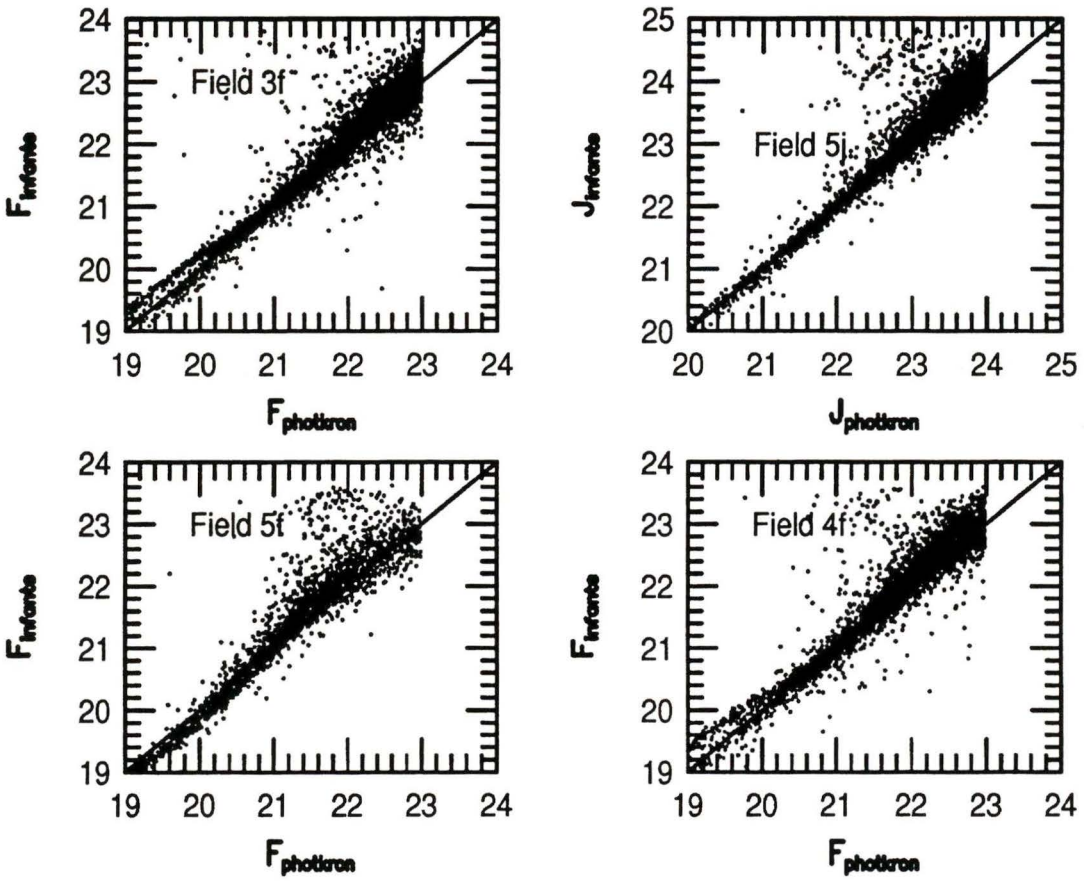

Figure 2.5: Photkron magnitudes, $J_{photkron}$, plotted against catngp magnitudes, $J_{infante}$, for field $5J$ and fields $3F$ - $5F$. The solid line has a gradient of 1. The photkron catalogue includes objects in the magnitude range $20 < J < 24$.

software.

Initial comparisons between catngp number counts and photkron number counts revealed that the former were significantly *higher* than the latter. However, the plots in Figures 2.4 and 2.5 indicate good photometric agreement between the two systems, indicating that the discrepancy is probably due to the *finding* algorithms rather than the photometry.

This view is supported by Figure 2.6. In this plot, number counts are plotted for the catngp data and for *only the photkron objects which matched catngp ones* (denoted by the triangles). This method eliminates spurious objects and tests specifically if differences in photometry are producing the number count discrepancy. In the matched plots the discrepancy is small. In addition, visual inspection of the excess population reveals it to be composed of lint and other spurious detections. This excess population of artificial objects is not a problem for us because, as will be explained in Chapter 3, all objects that are used to generate the correlation functions are manually inspected, a procedure which removes almost all spurious detections.

2.6.3 Adopted Zero Points

Table 2.3 shows the zero points which were determined from the calibration plots.

2.7 Making Matched Catalogues

We would also like to investigate how the colour of an object is related to its measured correlation. In astronomical terms, colour is calculated by

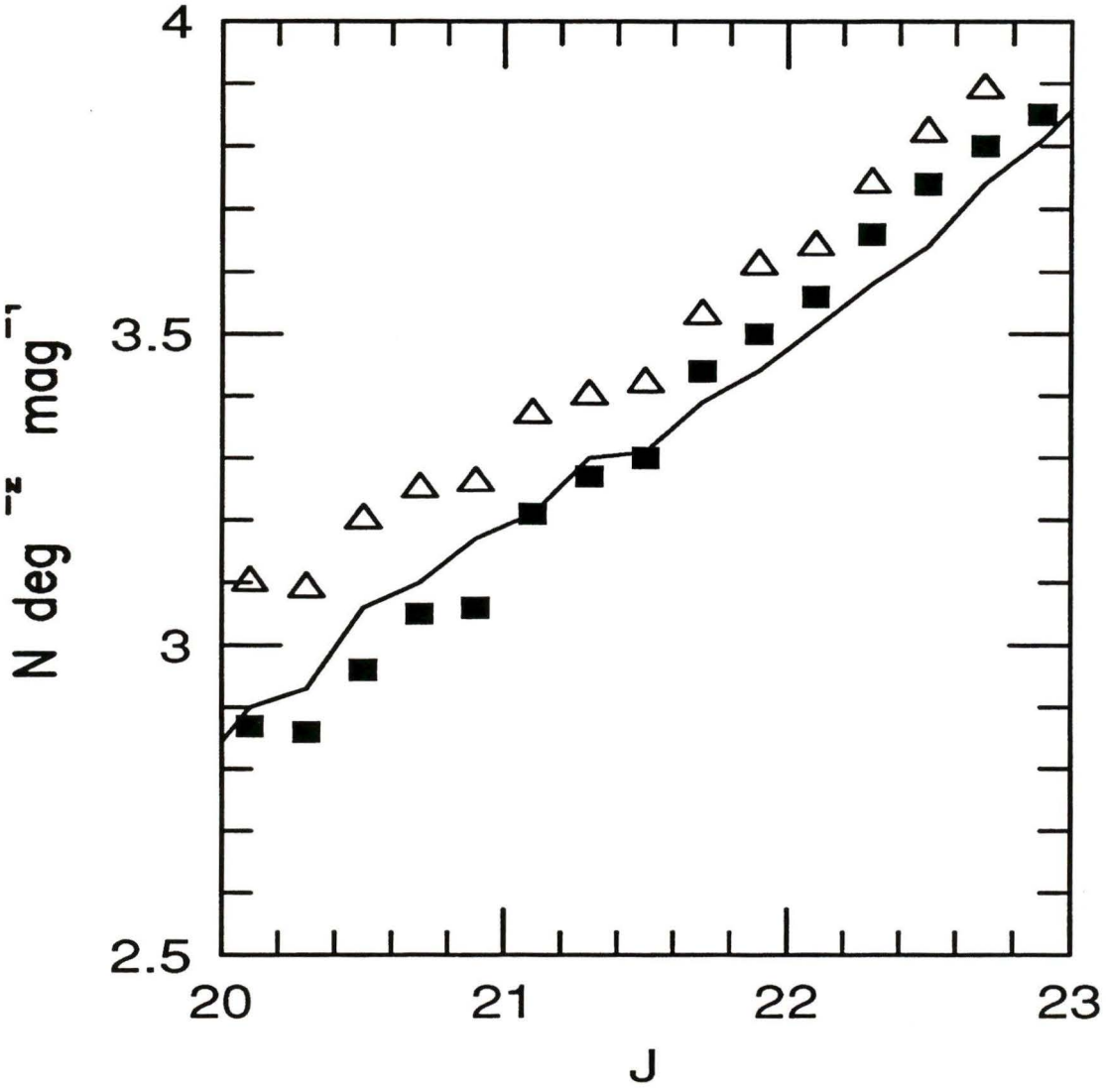

Figure 2.6: Number counts compared between catngp counts (solid line), photkron objects matched with catngp objects (squares) and the unmatched photkron catalog (open triangles)

Adopted Zero Points		
Frame	J-Band	F-Band
1	32.00	–
2	32.00	–
3	31.74	31.00
4	32.00	30.80
5	32.10	30.90

Table 2.3: Adopted zero points.

subtracting two magnitudes determined for an object in two different bandpasses; in our case, we will calculate a colour of $J - F$ from our J-band and F-band data. In order to do this, the co-ordinate transformation between the J-band plates and the F-band plates must be found, and objects matched between the two catalogues. To accomplish this we use the ten-term transformation introduced in Section 2.6. These coefficients provide a transformation between catngp – in either J or F raster systems; by applying the *reverse* transformation – raster to catngp–we may then use these coefficients to transform any arbitrary position in the F band co-ordinate system to the catngp system. By then applying the *forward* (J) transformation (as catngp J and F coordinate systems are the same) we may then transform to the raster J band.

2.8 Star/Galaxy Separation

To distinguish between stars and galaxies we used the "Inverse Second Moment" parameter which we introduced in Section 2.5. For each object this

quantity was plotted against apparent magnitude. Figure 2.7 is an example of such a plot. The stellar sequence, extending to the left, is clearly visible. To remove these objects, five points are marked on the graph defining a spline curve. Objects below this curve are rejected as stars and those above are retained as galaxies. Figure 2.8 shows Figure 2.7 after the stars have been rejected.

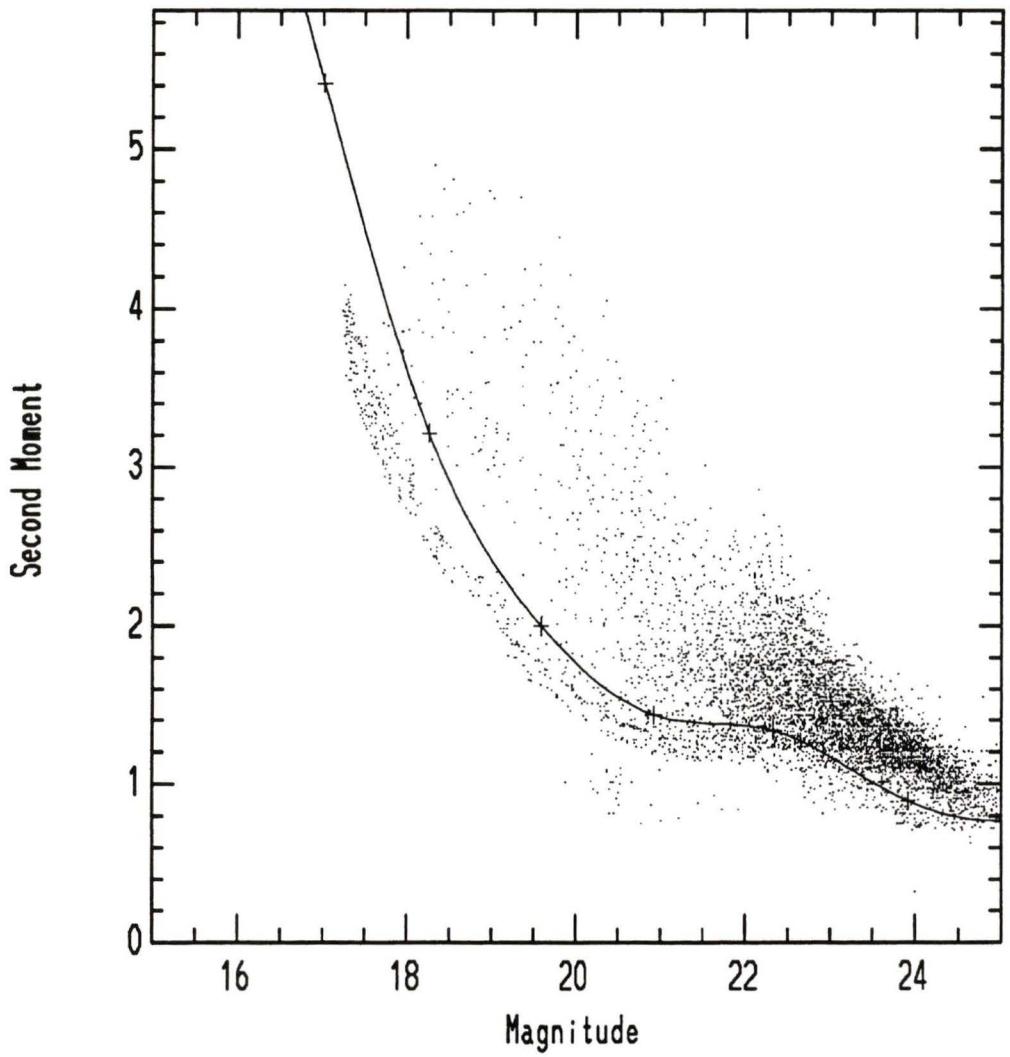

Figure 2.7: Plot of r_{-2} as a function of apparent magnitude for the 1J frame. The spline curve marked on the plot indicates the division between stellar and non-stellar regions.

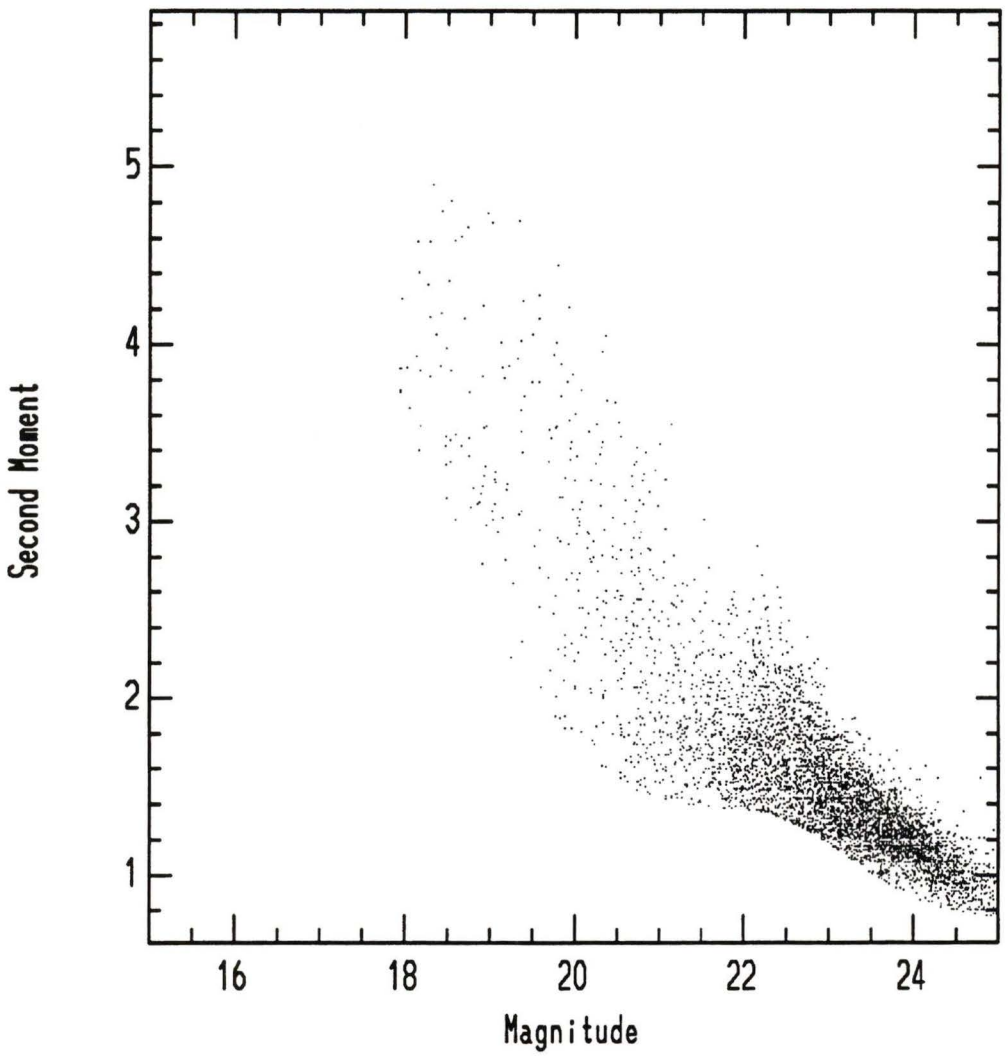

Figure 2.8: This is the same plot as before, but after the stars have been removed.

Chapter 3

Determining $\omega(\theta)$

3.1 Introduction

Now that we have produced a list of galaxies with positions and magnitudes our next task is to estimate their correlation function. In general terms, correlation function estimates proceed by two steps; first a *random* distribution of objects is generated, covering the same area as the detected objects. Next, the correlation function is derived by comparing this random (i.e, uncorrelated) distribution with the (correlated) objects. The precise estimator that we use for this task, and how it was chosen, is discussed below.

Estimating the correlation function can be a difficult process. Edge effects (caused by the finite size of the detection area), the geometry of the fields and errors in the photometry all can introduce systematic biases in the correlation amplitude. Fortunately for us, however, these effects are not significant at the scale we are most interested in (i.e., $1'' - 10''$). In Chapter 1 we described the correlation function's power-law behaviour which has been confirmed by many workers. At large angular separation the correla-

tion function has an extremely small amplitude (typically $10^{-2} - 10^{-3}$) and consequently the Signal-to-Noise (S/N) of correlation amplitudes is very low. To measure accurately $\omega(\theta)$ at these large separations careful attention to astrometric and photometric matters is required. Conversely, at the separation ranges we investigate, $\omega(\theta)$ is much larger– it may even be as large as 1-2. In this case, edge corrections become negligible. In addition, the method we used to estimate $\omega(\theta)$ greatly reduces edge effects by use of the N_{gr} estimator to calculate the pair density expected from a uncorrelated distribution. The practical implication of this is that we may safely measure correlation functions individually for each field, rather than transforming each field to a common co-ordinate system (for example, right ascension and declination) and calculating a global correlation function. This simplifies matters enormously.

To determine $\omega(\theta)$ we will calculate the correlation function for each for each of the fields (five in J and three in F) and then take the mean of $\omega(\theta)$ at each of the angular bins and assign the error in $\omega(\theta)$as the standard deviation of the mean of each of the angular bins. Alternative methods to calculate the errors, such as the bootstrap method, will also be discussed.

3.2 Choosing an Estimator of $\omega(\theta)$

To measure $\omega(\theta)$ we use the following formula:

$$1 + \omega(\theta_i) = \frac{N_r}{N_g - 1} \cdot \frac{N_{gg_i}}{N_{gr_i}} \cdot \frac{1}{B}, \tag{3.1}$$

where N_r represents the number of random objects generated, N_g is the num-

ber of galaxies in the sample, B is the "integral constraint" factor discussed below and N_{gg} and N_{gr_i} are the numbers of galaxy-galaxy and galaxy random pairs in the ith angular bin respectively. To reduce fluctuations in the angular correlation of the random catalogue (which scales approximately as $\sqrt{N_r}$) we will use a large number of random points–typically N_r is set to $10N_g$.

We must be extremely careful concerning how we generate our random numbers. Most system-supplied random numbers are not really random at all, but repeat with a frequency which would be noticeable with the large numbers of points which we must generate for our random comparison objects. To overcome these difficulties we use the `ran0` routine from *Numerical Recipes* (Press et al., 1986), which repeats over much longer intervals than the system-supplied routine. Random number generators also require a "seed"; if the same seed is chosen every time the program is invoked then the same sequence of (albeit random) numbers always results, which causes problems if correlation functions are to be calculated for many different fields. To avoid these problems a new seed is calculated from a varying quantity (such as the current time) each time the program is executed, ensuring that a different set of random numbers is always produced.

Notice that extra terms to account for edge effects are not included in this formula, for reasons discussed above. We may easily test that our estimator is free from biases by using it to calculate $\omega(\theta)$ for uncorrelated data–that is, random points as opposed to objects (magnitude zero point variations across the plate, which might produce a spurious correlation signal, were found to be negligible in the region we consider (Pritchet and Infante, 1992b)).

Our reasons for choosing this formula are as follows; firstly, this is the estimator used by Pritchet and Infante (Pritchet and Infante, 1992a; Pritchet and Infante, 1992b). A useful check on our work will be to compare our intermediate-separation correlation function with theirs. Agreement at these angular separations will be a useful test of our methods and improve our confidence in our results for the smaller-separation $\omega(\theta)$. Secondly, other estimators were tried and found not to give significantly different results from the one finally adopted.

In addition, note that what we describe is actually the sample's autocorrelation function. We are also interested in measuring the *cross*correlation function between disparate samples of objects. In this case, the number of objects at each angular separation is calculated by using either sample as a centre. A variant of the program used to calculate the autocorrelation function, called cc, computes these cross-correlations. Table 3.1 lists the different samples used in computing the cross correlation functions.

3.3 The Integral Constraint Term, B

The integral constraint term, B, is a constant which appears in the denominator of the angular correlation function expression. Its inclusion is necessary to correct for the finite measuring area of the plate; in this case, any power on small scales will result in $\omega(\theta) < 0$ for large θ. Over our sample, the correlation function must satisfy

$$\int \omega(\theta) d\Omega_1 d\Omega_2 = 0 \tag{3.2}$$

Sample Name	Description	Number (Fields 3,4,5)
apm?jf_all	All Objects	2948
apm?jf_b25	Bluest 25%	735
apm?jf_b50	Bluest 50%	1472
apm?jf_r25	Reddest 25%	738
apm?jf_r50	Reddest 50%	1475
apm?jf_all_b	Brightest Objects	242
apm?jf_b50_b	Brightest Bluest 50%	138
apm?jf_r50_b	Brightest Reddest 50%	104

Table 3.1: Samples used in generating the cross-correlation functions. These samples are all derived from the matched catalogues discussed in the previous section. Note that "all objects" are those which: i) have a magnitude in the range $19.5 < (J + F)/2 < 22.5$; ii) exist in a circular annulus centred on each of the frames. Furthermore, the "brightest" objects are those for which $19.5 < (J + F)/2 < 20.5$. The "?" in the sample name indicates either field 3,4,5; the numbers of objects quoted are total numbers of objects in these three fields.

Our sample will *not* satisfy this relationship without the addition of the integral constraint factor B. Our results do *not* depend critically on the value we choose for B, as the correlation function is so large at the small separations we are most interested in.

3.4 Editing the Object Catalogue

It would be hazardous to apply this estimator blindly to our data. For although measurement of the small angular separation $\omega(\theta)$ is not subject to errors which plague investigators of $\omega(\theta)$ on larger scales, there is still a very important effect which, unless accounted for, would produce a $\omega(\theta)$ very much larger than the true value. This effect arises from the spurious detections in the photometry catalogue. Many of the spurious detections are removed when photometry is performed; lint, scratches and so forth rarely will have a measured magnitude within the range of our catalogue. Moreover, most of these objects are uncorrelated and consequently will not cause any increase in correlation power. However, a significant class of spurious objects are those which involve multiple detections on bright, large objects such as stars or galaxies. For example, it is not inconceivable that "lumps" in the arms of spiral galaxies might be detected as discrete objects by our finding algorithm. These erroneous detections are particularly dangerous to us for two very important reasons; firstly, many have magnitudes within the magnitude limits of our catalogues; and secondly, they are strongly correlated– there are many galaxies in our catalogue whose angular extent is comparable to the size of the bins at which we measure the correlation functions. If

multiple detections on such objects were to go unchecked then the amplitude of the correlation function at these separations would be strongly biased.

To correct for this problem the following procedure is carried out for each field. Firstly, the photometry file containing all the objects within a specified magnitude range is read in, considering only objects within a circle centred on the plate centre, to alleviate any effects caused by the frame edges. Secondly, all the pairs within a given range of separations are found and their positions recorded. This list is sorted, and then degenerate pairs are removed so that each pair contains at least one unique object, for the purposes of inspection (these pairs are kept when the correlation function is computed). Next, the image of the field is displayed and the location of all the pairs are marked on it using the IRAF task **tvmark**. Each pair may be then examined individually. If either of the objects in the pair is found to be spurious it is marked and its line number in the photometry file is written to disk. When the correlation function is next computed the line number of each object read in is compared with the line numbers of spurious objects and if they are the same, the object is discarded. In addition, provision is made for excising small regions from each scan. Such excised regions generally contain saturated stars which have many spurious detections. In these ways the accuracy of the computed correlation function may be greatly improved.

3.5 Determining Errors in $\omega(\theta)$

3.5.1 Poissonian Error Estimates

This is the simplest and most commonly used method used to estimate errors in $\omega(\theta)$. It presumes that measurement angular correlation function is a Poisson counting process. In this case, the error in each of angular bins is $\propto \frac{1}{N}$ where N is the number of objects in the bin. All these errors are then added in quadrature over all available fields, i.e., if σ_1 and σ_2 are two error estimates, then the total error is given as $\sigma_t^2 = \sigma_1^2 + \sigma_2^2$).

3.5.2 Statistical Error Estimates

Another method is open to us as we have measurements of $\omega(\theta)$ in several fields. The error in $\omega(\theta)$ may be calculated directly as the standard deviation of $\omega(\theta)$ over all fields, i.e., $\frac{\sigma_t = \sigma}{\sqrt{(N)}}$. We prefer this method to the above one as it more sensitive to field-to-field variations in $\omega(\theta)$. In most cases, however, error bars are approximately the same as those calculated from the method presented in Section 3.5.1

Chapter 4

Results

4.1 Final Characteristics of the Catalogues

The final J band catalogue has 6192 galaxies in the magnitude range $20 < J < 23$ and covers an area of 0.87 deg^2, whereas the F band catalogue has 4160 galaxies in the magnitude range $19 < F < 22$ over an area of 0.52 deg^2. The matched catalogue contains 2795 objects in the range $19.5 < \left(\frac{J+F}{2}\right) < 22.5$ and also covers 0.52 deg^2. The total area available was smaller that in Pritchet and Infante (1992a; 1992b; 1995) because only the central regions of the plates were scanned and because the catalogues generated from each plate have circular boundaries in order to minimise the noise in $\omega(\theta)$ generated by edge effects, to permit comparisons with the Pritchet and Infante correlation functions.

4.2 Pair Fraction Calculations

A simple way to test if an excess exists in counts of closely separated objects is to compute the ratio of the number of objects at a certain (larger separation)

bin with the number in some smaller separation bin. This ratio may then be compared with the ratio expected from the correlation function appropriate to that sample (at large separations). The results from such a study should be broadly consistent with a direct examination of the correlation function.

We follow the example of Carlberg et al. (1994), who choose an inner bin of $1'' < \theta < 6''$ and an outer bin of $6'' < \theta < 24''$. This enables us to compare results from our sample of ~ 6000 galaxies with those derived from their much smaller sample of only ~ 300 galaxies.

To compare the ratio of pairs found in two angular separation bins with the ratio predicted by extrapolating the Infante & Pritchet (1995) correlation function to smaller separations, we must first derive an expression for the number of pairs separated by θ,

$$n_p = \frac{1}{2} N^2 < \delta\Omega > [1 + \omega(\theta)] \tag{4.1}$$

where N is the number of objects $\deg^{-2}$, Ω is the solid angle subtended, and $\omega(\theta)$ is the angular correlation function. To get the *total* number of pairs in a range of angular separations, N_p, we must integrate the product of equation 4.1 and an annular segment, $2\pi\theta$ over this range, i.e., compute

$$N_p = \frac{1}{2} N^2 \int_{\theta_1}^{\theta_2} [1 + \omega(\theta)] 2\pi\theta d\theta \tag{4.2}$$

From this equation we may then easily compute the pair ratio for different angular separations. The pair ratio $N_p(3'' - 6'')/N_p(6'' - 24'')$ is computed using the fits to the angular correlation function given in Pritchet & Infante (1995) appropriate to the sample under investigation. For the $20 < J < 23$

sample, using $A_\omega^{\delta=0.8}(1') = 0.045$ (this notation means that at an angular separation of 1′ for a power-law of slope -0.8, $\omega(\theta) = 0.045$) we find that $N_p(6'' - 24'')/N_p(3'' - 6'') = 16.7$. The *observed* value for this pair ratio is 17.1 ± 1.7 from our data.

Similarly, for the F band, using $A_\omega^{\delta=0.66}(1') = 0.083$, we find that $N_p(6'' - 24'')/N_p(3'' - 6'') = 16.53$. The observed value for this pair ratio is 17.7 ± 2.5. For the merged catalogue, we use $A_\omega^{\delta=0.66}(1') = 0.054$ and find the pair ratio is 17.57, compared to an observed value of 18.5 ± 6.0.

These results are summarised in Table 4.1, as well as results for the pair fractions $N_p(6'' - 24'')/N_p(1'' - 6'')$ as observed for all catalogues and as derived using the same parameters for the correlation function as the other pair fractions. These results are probably less reliable than the $N_p(6'' - 24'')/N_p(3'' - 6'')$ pair fractions as a consequence of incompleteness at the smallest separations.

In addition, one may compute the ratio of number of galaxies in small separation pairs to the total numbers of galaxies in our sample. The value for this fraction in the $z = 0$ galaxy population is 4%. This number may be derived by considering local galaxy samples such as the UGC catalogue and projecting our 6″ separation criterion to the local sample.

Comparing our results to that of Carlberg et al., we find that in the J band catalogue there are 528 galaxies in pairs with $\theta < 6''$. This corresponds to a pair fraction (i.e, the number of galaxies which are in pairs separated by less than this amount as a percentage of the total number of galaxies in the catalogue) of $8.5\% \pm 0.3\%$.

In the F band catalogue there are 368 galaxies with $\theta < 6''$, correspond-

Quantity	J cat	F cat	Merged cat
Total Number of Galaxies	6192	4160	2795
$N_p(1'' - 6'')$	264	184	83
$N_p(3'' - 6'')$	182	133	60
$N_p(6'' - 24'')$	3105	2348	1108
$N_p(6'' - 24'')/N_p(1'' - 6'')$	11.76 ± 0.57	12.76 ± 0.95	13.4 ± 2.3
$N_p(6'' - 24'')/N_p(1'' - 6'')$[derived]	12.24	12.14	13.15
$N_p(6'' - 24'')/N_p(3'' - 6'')$	17.1 ± 1.7	17.7 ± 2.5	18.5 ± 6.0
$N_p(6'' - 24'')/N_p(3'' - 6'')$[derived]	16.73	16.53	17.57

Table 4.1: Numbers of pairs in three angular separation bins, $1'' - 6''$, $3'' - 6''$ and $6'' - 24''$. The ratio of pair counts at large separations compared with counts at smaller separations is computed, in addition to the ratios expected from the Pritchet and Infante correlation functions. Error bars for the observed quantities were computed using Poisson counting statistics.

ing in this case to a pair fraction of $8.8\% \pm 0.5\%$. In the merged catalogue we find there are 166 galaxies separated by less than $6''$, giving a pair fraction of $5.6\% \pm 0.5\%$.

4.3 Autocorrelations in the Unmatched Catalogues

We will first consider the autocorrelation function (where "autocorrelation" describes the correlation of a sample *with itself*. Later we will consider the *cross*-correlation function of the samples, which gives the correlations between two samples). Figure 4.1 shows the autocorrelation function computed from the J band data. Objects are selected in the magnitude range $20 < J < 23$. The correlation function is determined for each of the five fields

(1J, 2J, 3J, 4J, 5J) and an average is taken. Error bars for this and all subsequent correlation function plots were calculated from the standard deviation of $\omega(\theta)$ over all available fields. In addition, a *global* correlation function was computed by adding up all the object counts at the various separations over all the fields. This was found not to differ from the local estimates. The solid line shows a fit to the Pritchet and Infante (1995) correlation function for objects with the same range in magnitudes and with $A_\omega^{\delta=0.8} = 0.045$. As is apparent from the plot, $\omega(\theta)$ does not deviate significantly from the Infante and Pritchet correlation functions, even at small separations. This is in agreement with the results from the pair count ratios already presented.

Figure 4.2 shows the autocorrelation function computed from the F band data. Objects are selected in a magnitude slice $19 < F < 22$ and the correlation function is averaged over the three available fields. As before, the solid line represents a fit to the Infante and Pritchet correlation function over the same magnitude range for their sample with $A_\omega^{\delta=0.66} = 0.045$.

4.4 Autocorrelations in the Matched Catalogue

Investigating the correlation functions of the merged catalogue provides an important test of the methods outlined above. The matched catalogue was generated using different software than the unmatched catalogue, and the correlation function was measured using a program designed specifically for use with this catalogue. It is for these reasons that the results from the matched catalogues form an important consistency check on the results from

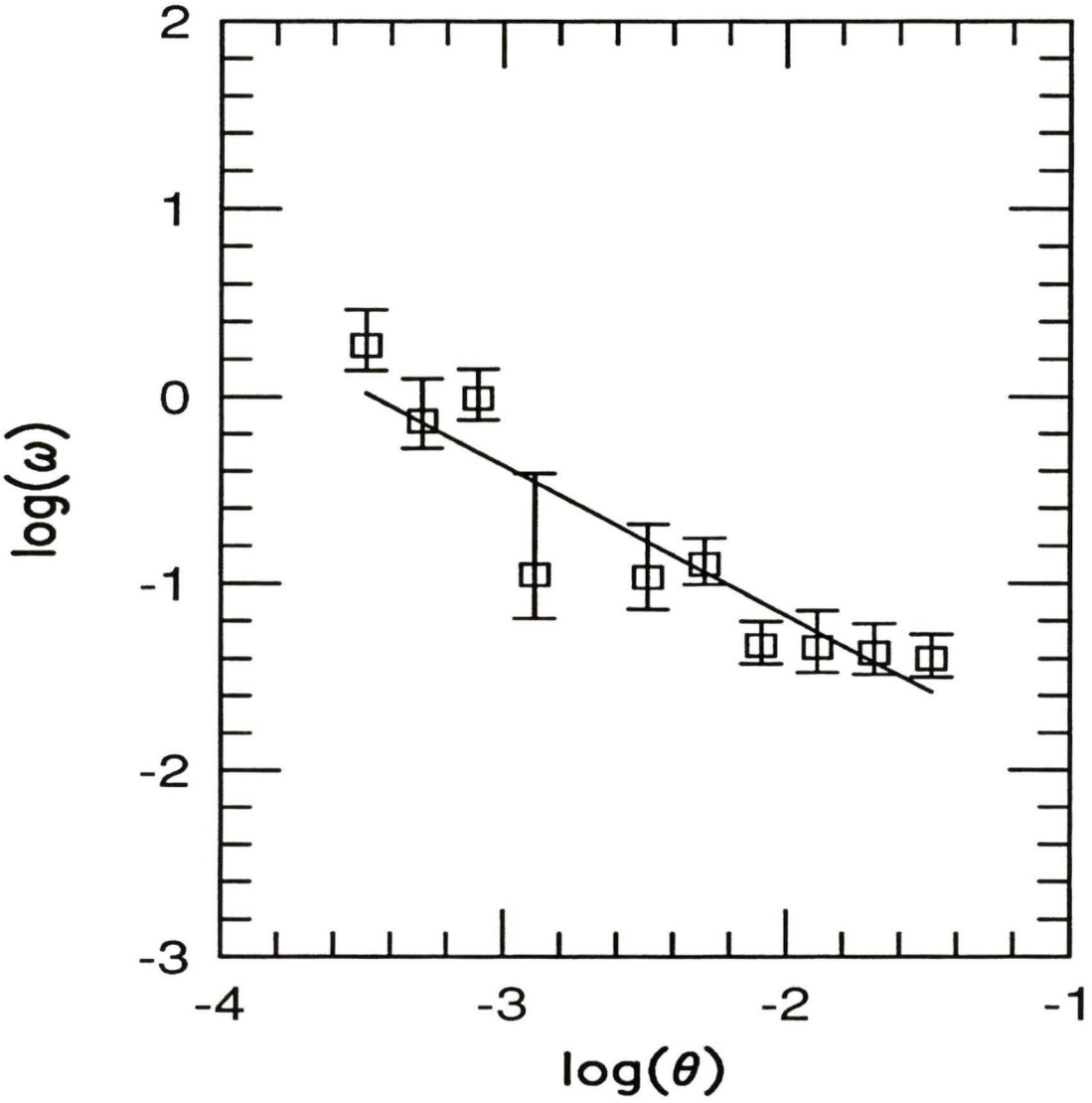

Figure 4.1: The autocorrelation ω of galaxies as a function of angular separation θ for the unmatched J-band data. The solid line represents a fit to the Infante and Pritchet (1995) correlation function for this bandpass and magnitude range and with amplitude and slope $A_{\omega}^{\delta=0.8} = 0.045$.

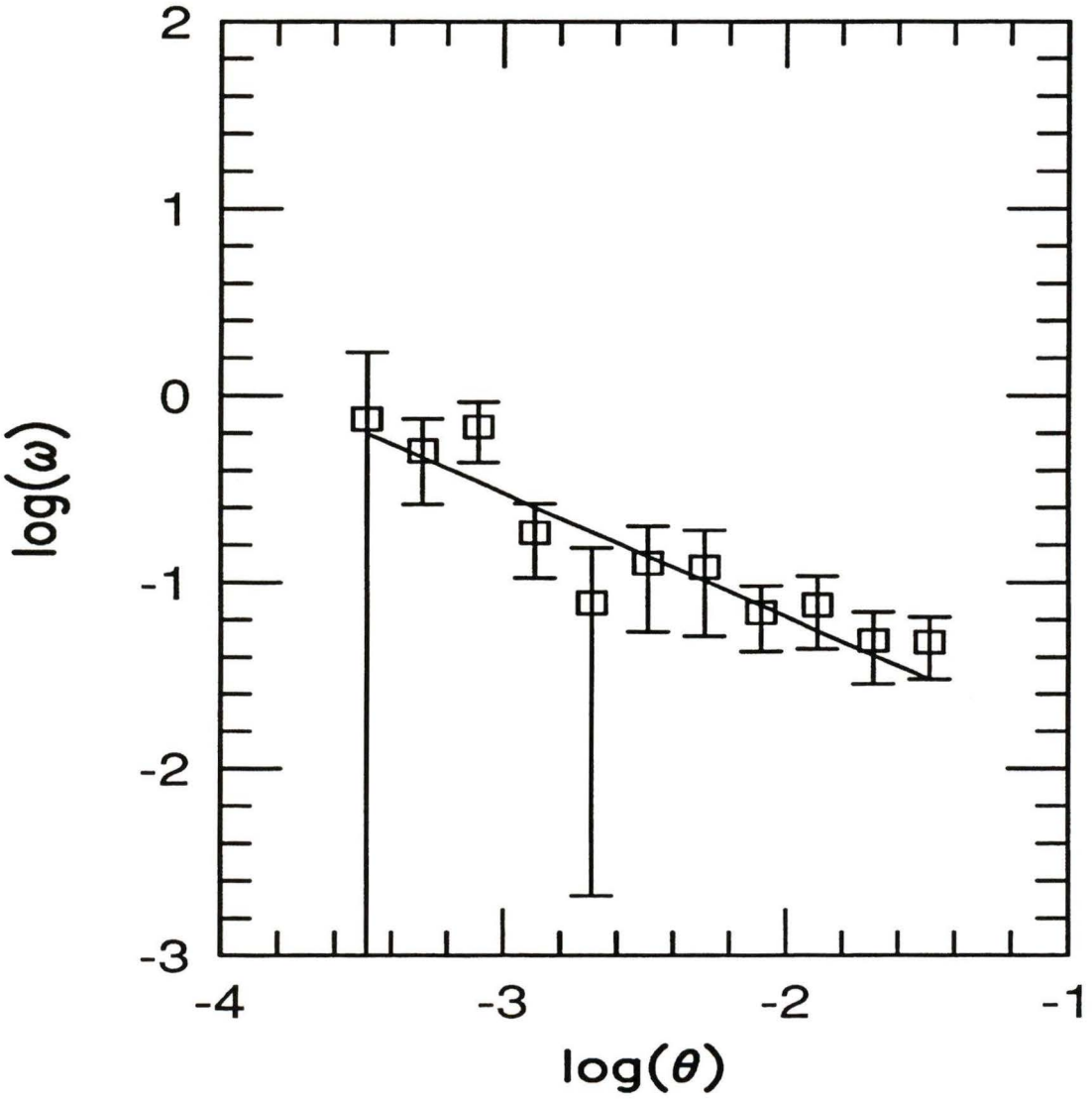

Figure 4.2: The autocorrelation ω of galaxies as a function of angular separation θ for the unmatched F-band data. The solid line represents a fit to the Infante and Pritchet (1995) correlation function for this bandpass and magnitude range and with amplitude and slope $A_\omega^{\delta=0.66} = 0.045$.

the unmatched data.

Figure 4.3 shows the autocorrelation function for the entire matched catalogue, averaged over three fields for which both J and F band colours are available. Error bars represent the standard deviation of the correlation function over the three fields (divided by $\sqrt{N}$, where N is the number of fields). The solid line represents a fit to the Infante and Pritchet (1995) correlation function for the magnitude range $20 < \left(\frac{J+F}{2}\right) < 23$. Note that this magnitude range is *not* the same as the magnitude range of objects in the matched catalogue, which is $19.5 < \left(\frac{J+F}{2}\right) < 22.5$. This slight mis-match in magnitude ranges has the effect of producing slightly *higher* correlation amplitudes in the current matched catalogue, although this is not noticeable in the figures.

Figure 4.3 shows the autocorrelation function for the entire matched catalogue, averaged over three fields for which both J and F band colours are available. Error bars represent the standard deviation of the correlation function over the three fields.

Similarly, Figures 4.4 and 4.5 show the autocorrelation functions for the reddest and bluest 25% of galaxies respectively, whilst the correlation function for the reddest and bluest 50% of galaxies is shown in figures 4.6 and 4.7. Furthermore, there is slight evidence that both the red and blue samples show an excess in correlation power at small separations.

It is interesting to note that the correlation power for the red sample is considerably higher than for the blue sample. This will be discussed further in Section 5.3.

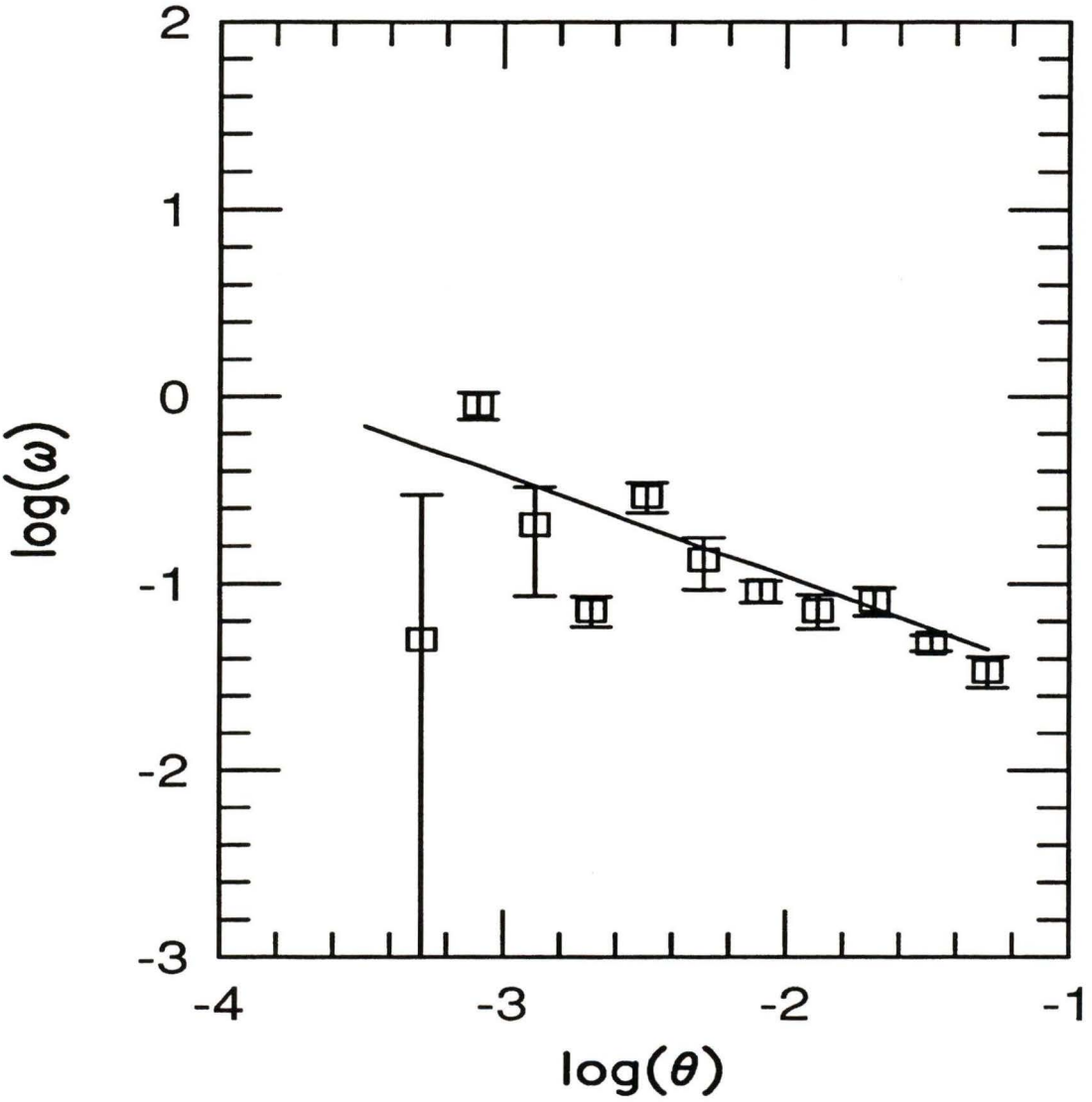

Figure 4.3: The autocorrelation ω of galaxies as a function of angular separation θ for the matched data. The solid line represents a fit to the Infante and Pritchet (1995) correlation function for their merged catalogue with amplitude and slope $A_\omega^{\delta=0.54}(1') = 0.083$ and covering the magnitude range $20 < \left(\frac{J+F}{2}\right) < 23$.

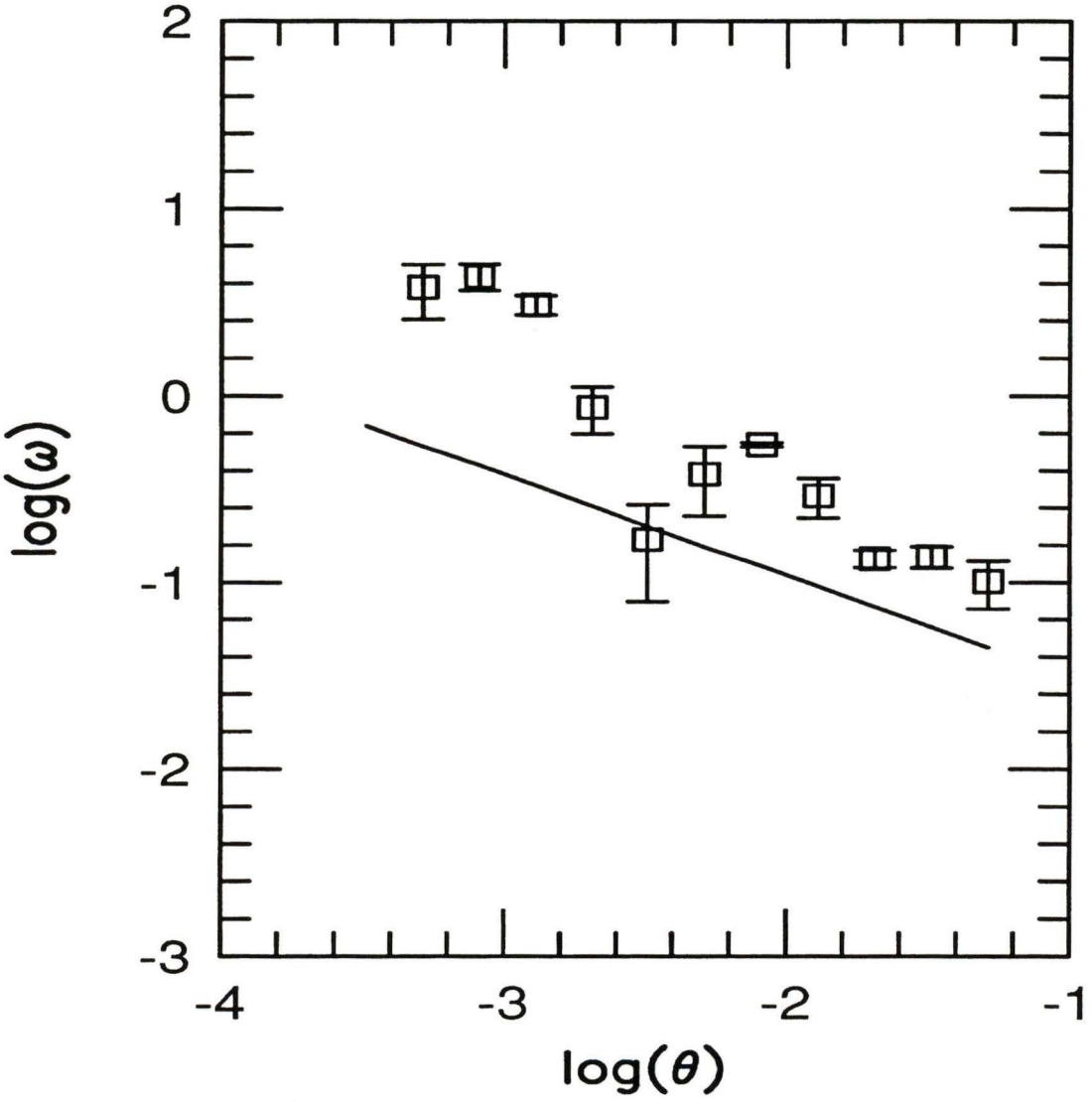

Figure 4.4: The autocorrelation ω of the reddest 25% of galaxies as a function of angular separation θ for the matched data. The solid line represents a fit to the Infante and Pritchet (1995) correlation function for their merged catalogue with amplitude and slope $A_{\omega}^{\delta=0.54}(1') = 0.083$ and covering the magnitude range $20 < \left(\frac{J+F}{2}\right) < 23$.

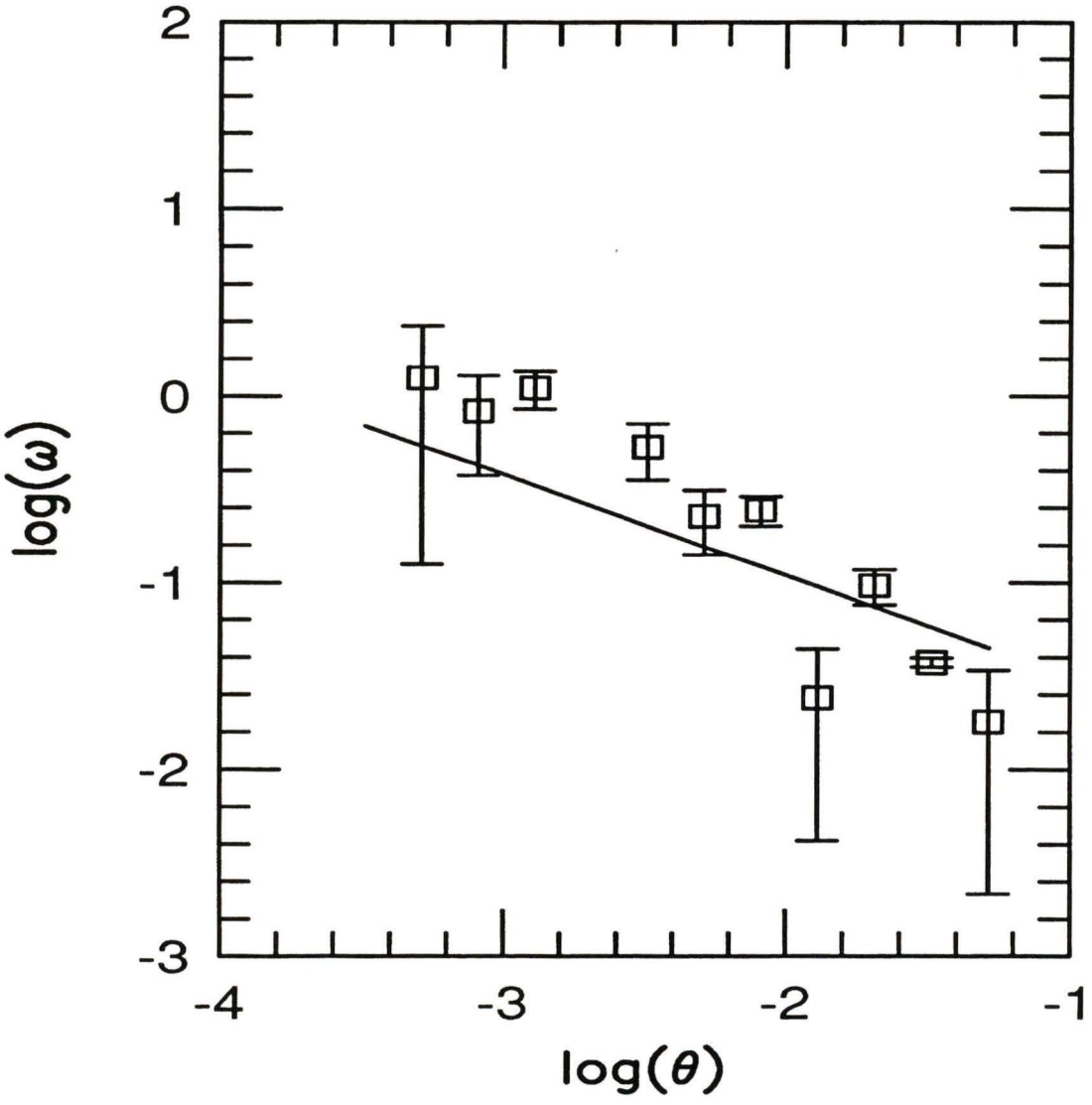

Figure 4.5: The autocorrelation ω of the bluest 25% of galaxies as a function of angular separation θ for the matched data. The solid line represents a fit to the Infante and Pritchet (1995) correlation function for their merged catalogue with amplitude and slope $A_{\omega}^{\delta=0.54}(1') = 0.083$ and covering the magnitude range $20 < \left(\frac{J+F}{2}\right) < 23$.

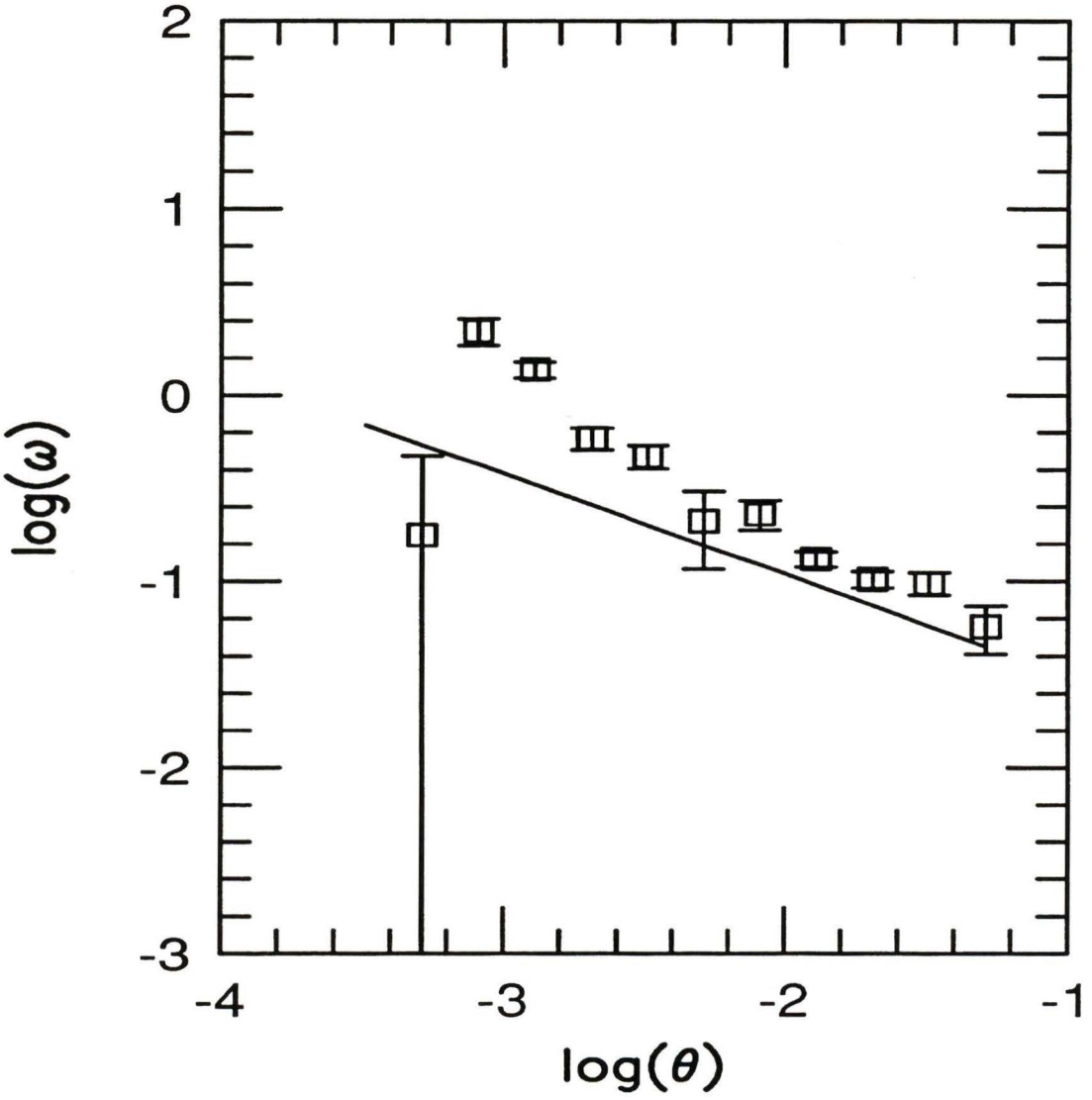

Figure 4.6: The autocorrelation ω of the reddest 50% of galaxies as a function of angular separation θ for the matched data. The solid line represents a fit to the Infante and Pritchet (1995) correlation function for their merged catalogue with amplitude and slope $A_{\omega}^{\delta=0.54}(1') = 0.083$ and covering the magnitude range $20 < \left(\frac{J+F}{2}\right) < 23$.

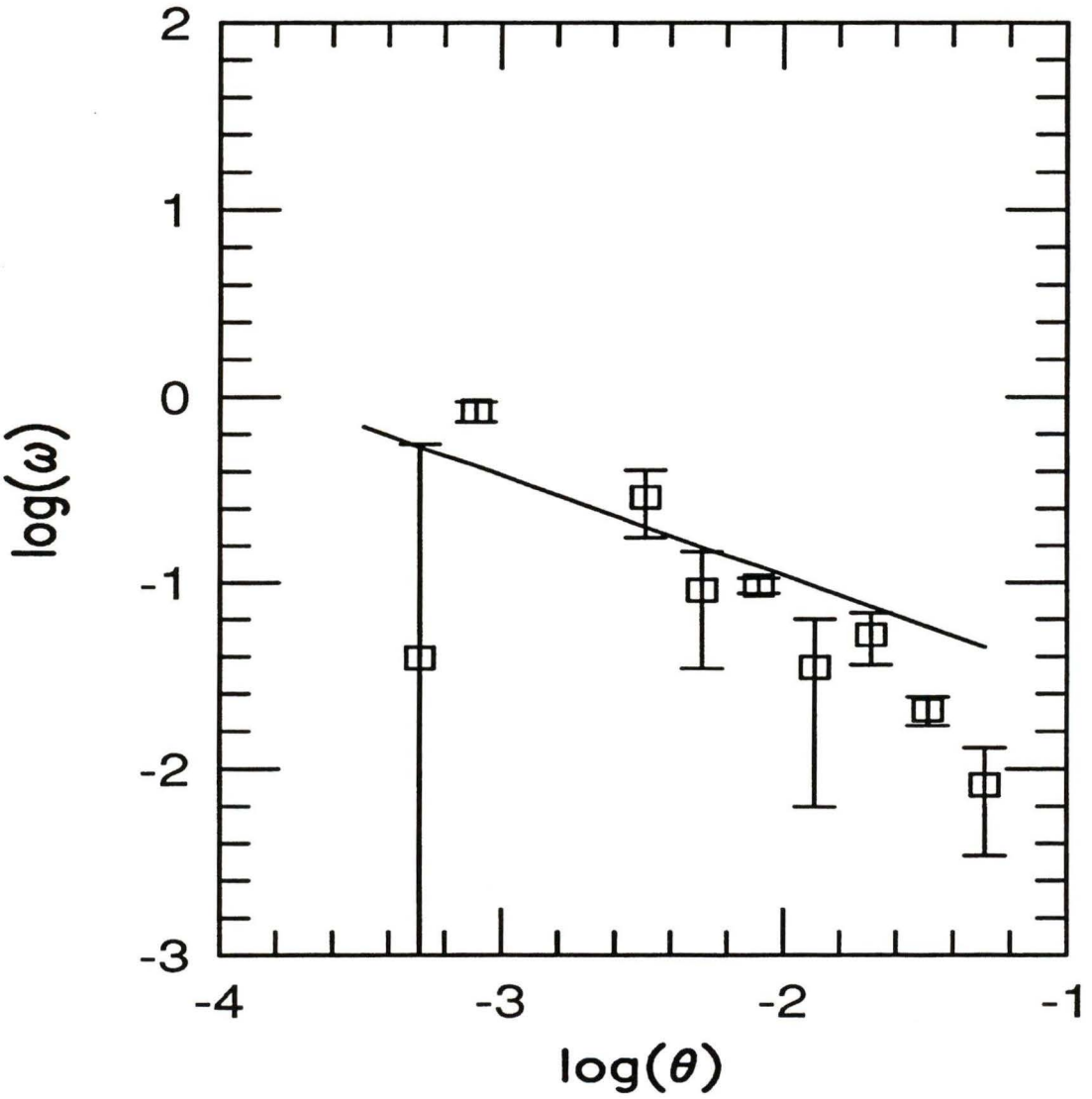

Figure 4.7: The autocorrelation ω of the bluest 50% of galaxies as a function of angular separation θ for the matched data. The solid line represents a fit to the Infante and Pritchet (1995) correlation function for their merged catalogue with amplitude and slope $A_{\omega}^{\delta=0.54}(1') = 0.083$ and covering the magnitude range $20 < \left(\frac{J+F}{2}\right) < 23$.

4.5 Pair Properties

If pairs were undergoing merging events then one would expect paired objects to have different properties than field objects. One such difference would be bluer colours as a result of increased star-formation triggered by the merging event. Another might be an anomalously small difference in magnitude or colour between the paired objects or the existence of emission-line features in their spectra, e.g., [OII] lines (again as consequence of merging or interactions). Conversely, Cowie et. al, (1994) predict that starbursting episodes in galaxy histories produces many small blue galaxies surrounding larger, parent galaxies, a prediction which we shall test by measuring cross-correlation functions in Section 4.6.

A number of studies (Carlberg et al., 1994; Zepf and Koo, 1989), in addition to the present one, have attempted to determine how pairs differ from field galaxy population. Most have reported no difference between the field population and the paired population. This null result has several explanations (Carlberg et al., 1994); first, if the *field* population has recently ($<$ 3Gyr ago) undergone merging then it would not appear different from a merging pair population. Secondly, the pair and field colour difference is expected to be only $\sim$ 10% (Carlberg et al., 1994; Shanks et al., 1980) which is difficult to detect with photographic or CCD photometry, given the huge range in galaxy colours. Thirdly, because we measure the *projected* pair count on the sky, rather than the actual pair count, our bins are contaminated by objects which are not physically associated or even objects that *are* physically associated but which are not interacting and will not merge.

Several samples were created in an attempt to determine if differences exist between the colour of the pair and field populations. The simplest test to perform is to investigate how the mean pair colour varies as a function of the angular separation of its members. This is illustrated in Figure 4.8. In each of the bins the mean colour is computed and this is plotted against angular separation. The bins are logarithmically spaced, and are identical to those used in the computation of the angular correlation function. Error bars correspond to the standard deviation in mean colour at each of the bins. As can be seen from this plot, there is no (statistically significant) evidence that the mean colour of a paired object is any different from the field object colour.

It would be better, however, to investigate the bluest or reddest object in a pair; if red objects were paired with blue objects then the mean colour of both objects would not be significantly different from the field. To address these issues in Figure 4.9 the colour of the bluest object in a pair is plotted against the angular separation of objects in the pair for two samples; one for which $6'' < \theta < 24''$ (representing the field population) and one for which $1'' < \theta < 6''$ (representing the excess population). In this case, a slight difference is found between the mean colour of the galaxies which are separated by small amounts ($1'' < \theta < 6''$) and those which are separated by larger amounts. The mean colour of galaxies in the inner bin is found to be 1.07, with an error in the mean of 0.03, whilst in the outer bin the mean colour is 0.98 and the standard deviation 0.01, i.e., the inner bins are slightly redder than the outer bins. The same conclusions are drawn if one studies the *reddest* paired objects, where the mean colour in the inner bin is found

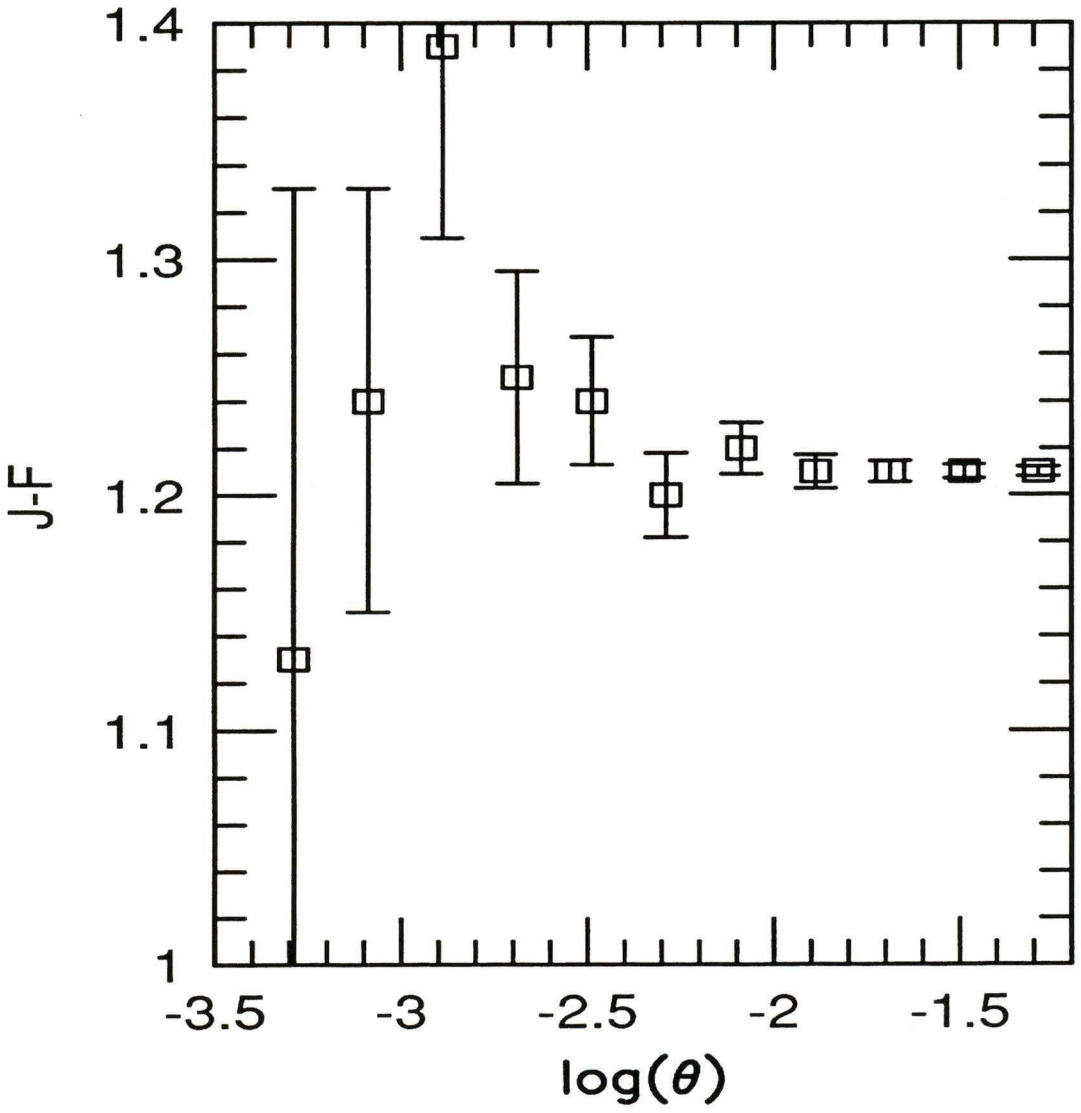

Figure 4.8: Mean pair colour, expressed as $J - F$, as a function of angular separation, θ, for all the objects in the matched catalog. Error bars are computed from the standard deviation of $J - F$ at each bin.

to be 1.50 with an error in the mean of 0.03, whilst in the outer bin the mean colour is 1.44 with an error in the mean of 0.01. These results are presented in Figure 4.9, Figure 4.10 and Figure 4.11.

Finally, we may investigate how the *difference* in colour of objects in pairs depends on angular separation. Once again, two samples are created; a small separation one (in which, as before, $1'' < \theta < 6''$) and a larger separation one for which $6'' < \theta < 24''$. The difference in colour as a function of angular separation for these two samples is plotted in Figure 4.11. The mean of the colour difference for the inner sample is 0.22 with an error in the mean of 0.03, whilst the outer sample has a mean of 0.23 with a standard deviation of 0.01, i.e., no difference between pair and field populations. These results are summarised in Table 4.2.

Sample Selection	$< J - F >_{1''-6''}$	$< J - F >_{6''-24''}$
Reddest Object	1.50 ± 0.03	1.44 ± 0.01
Bluest Object	1.06 ± 0.03	0.98 ± 0.01
Brightest Object	0.50 ± 0.03	0.43 ± 0.01
Dimmest Object	1.23 ± 0.02	1.09 ± 0.01
Colour Difference	0.22 ± 0.03	0.23 ± 0.01

Table 4.2: The mean colour of paired objects, where each object is selected from the pair by the indicated criterion. Mean colours are given for both an inner bin and an outer bin. Error bars quoted correspond to the error in the mean.

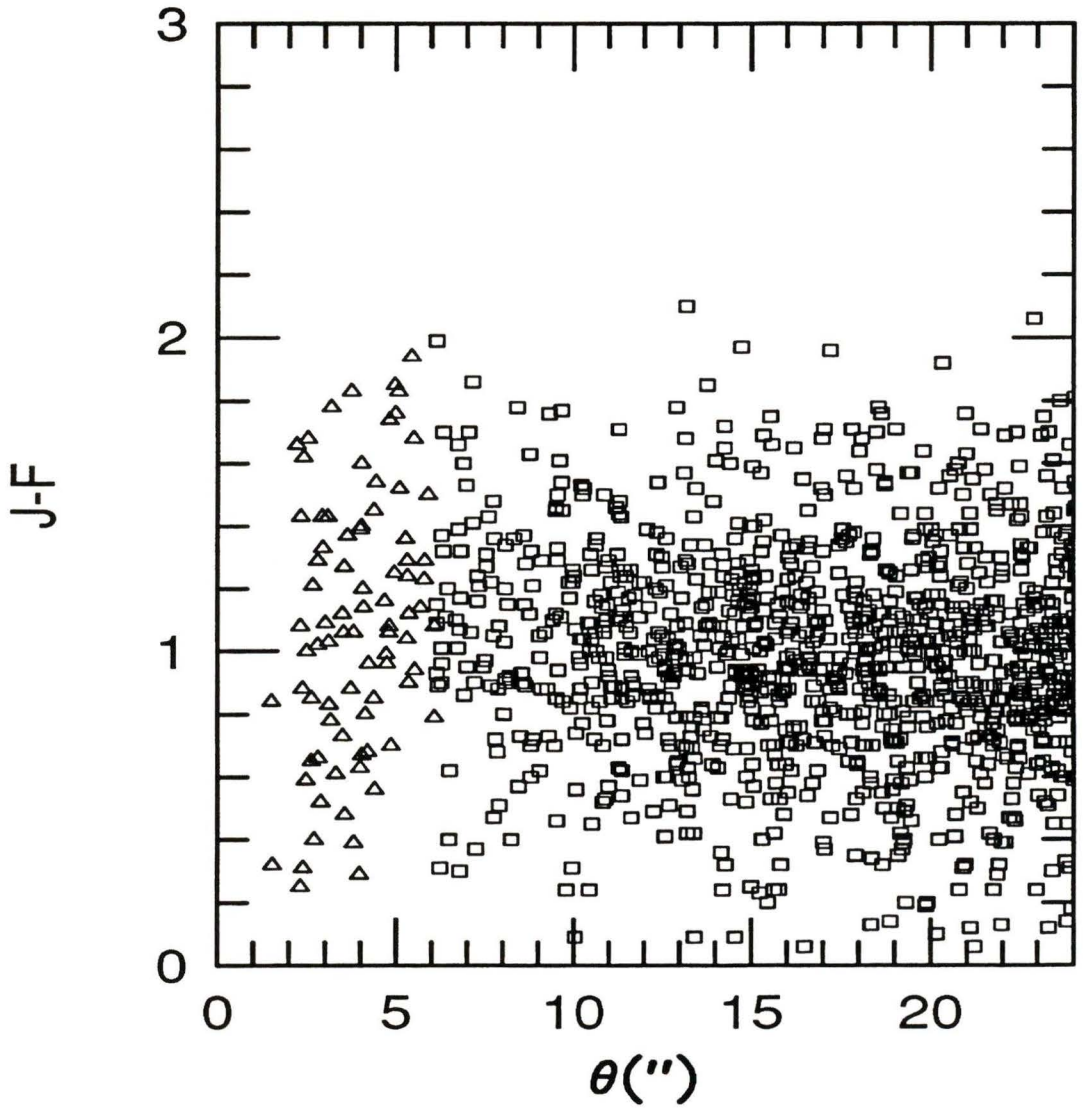

Figure 4.9: The colour, $J - F$, of the bluest galaxy in a pair plotted as a function of angular separation θ for two ranges of separations, $6'' < \theta < 24''$ (open squares) and $1'' < \theta < 6''$ (open triangles).

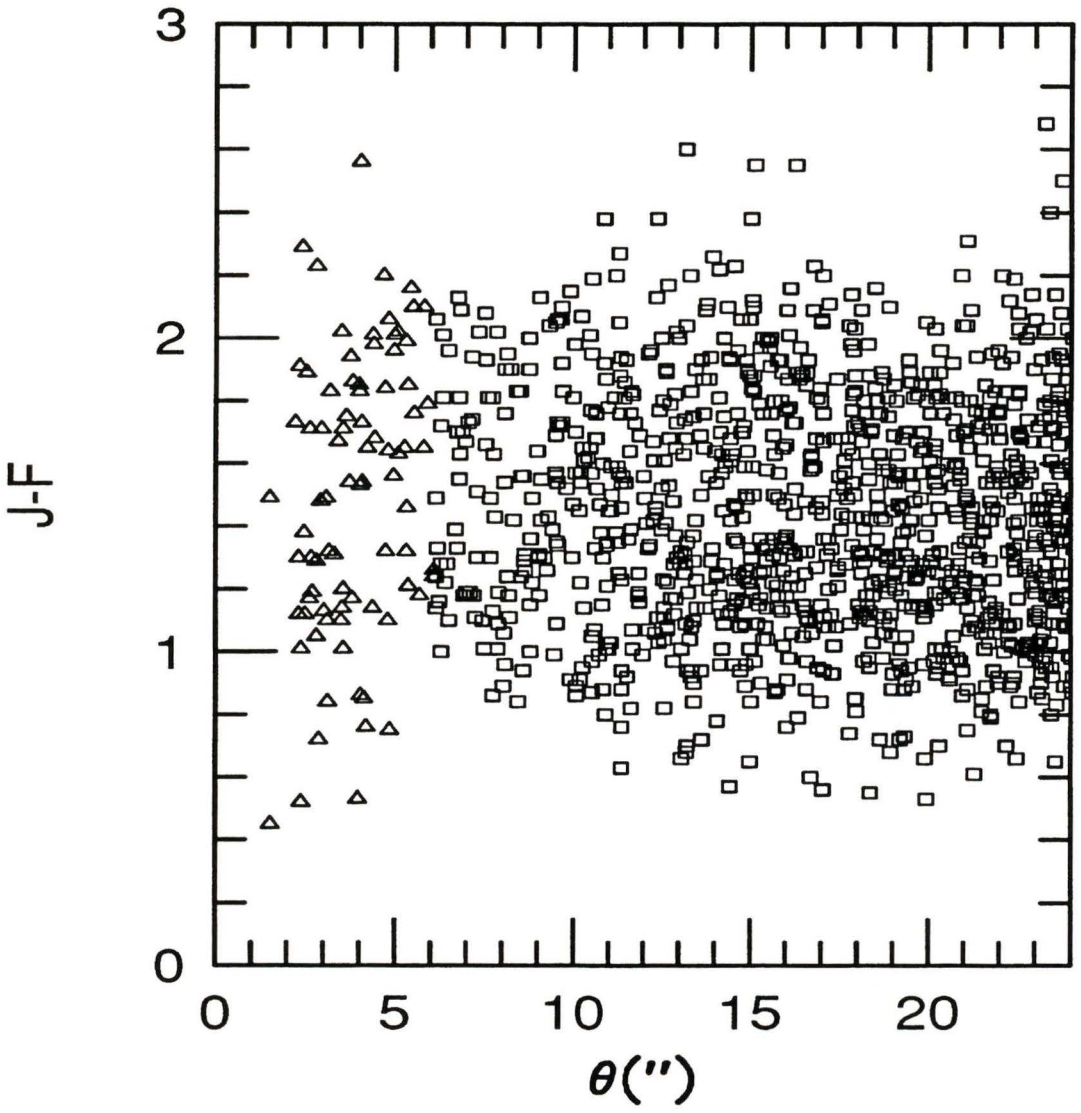

Figure 4.10: The colour, $J - F$, of the reddest galaxy in a pair plotted as a function of angular separation θ for two ranges of separations, $6'' < \theta < 24''$ (open squares) and $1'' < \theta < 6''$ (open triangles).

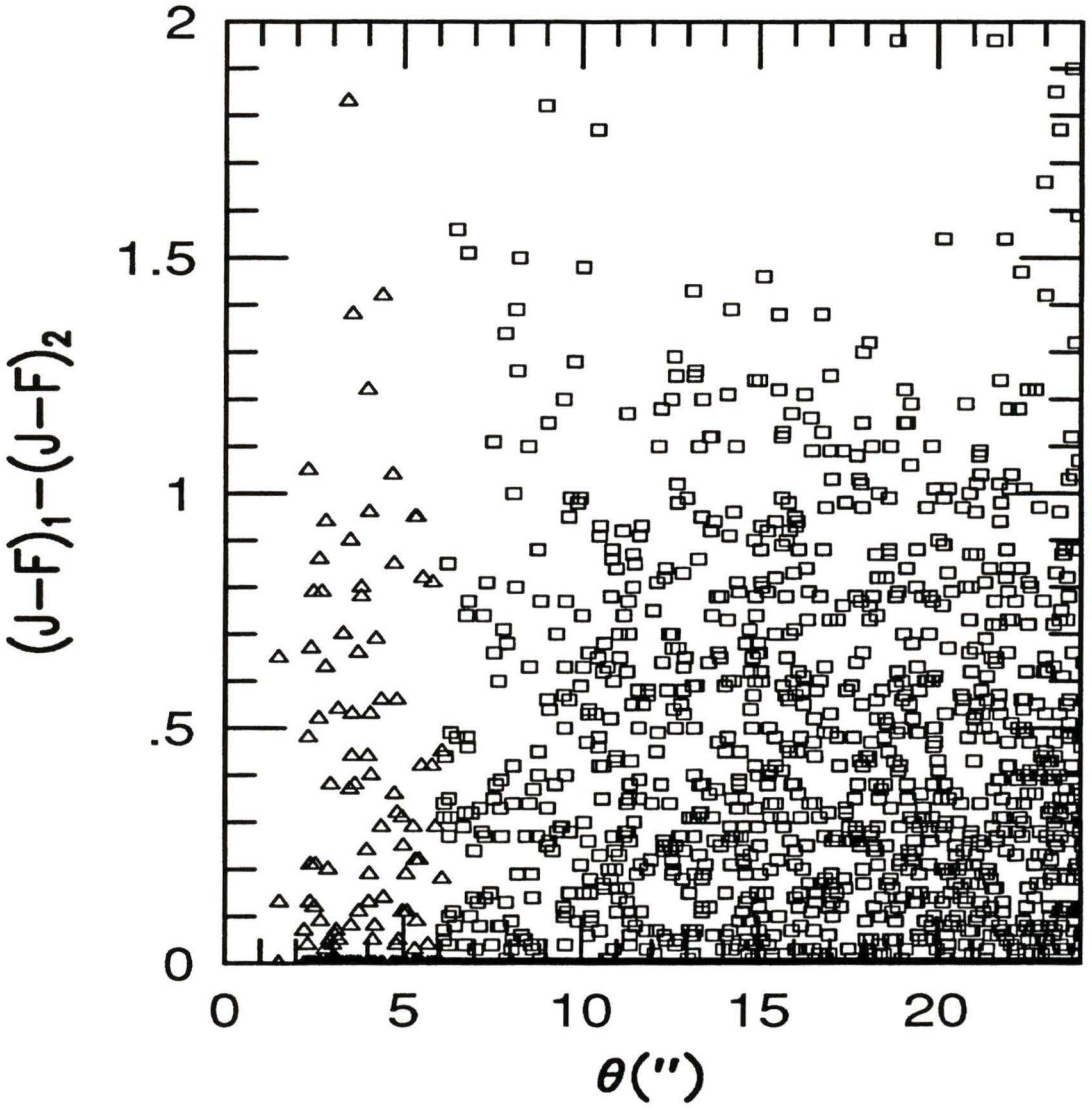

Figure 4.11: The difference in colour, $(J-F)_1-(J-F)_2$, of paired objects as a function of angular separation θ for two ranges of separations, $6'' < \theta < 24''$ (open squares) and $1'' < \theta < 6''$ (open triangles).

4.6 Cross Correlations in the Merged Catalogues

Figure 4.12 shows the cross-correlation function ω of bright galaxies with the entire sample. The solid line represents the Pritchet and Infante correlation function for their merged catalogue. The filled triangles represent the auto-correlation of the bright sample. Notice that there is some evidence that the cross-correlation function for the *entire* sample has a slightly higher amplitude for the inner bins than the bright-bright correlation. In addition, slope of the cross-correlation function is steeper than the slope of the bright-bright correlation function.

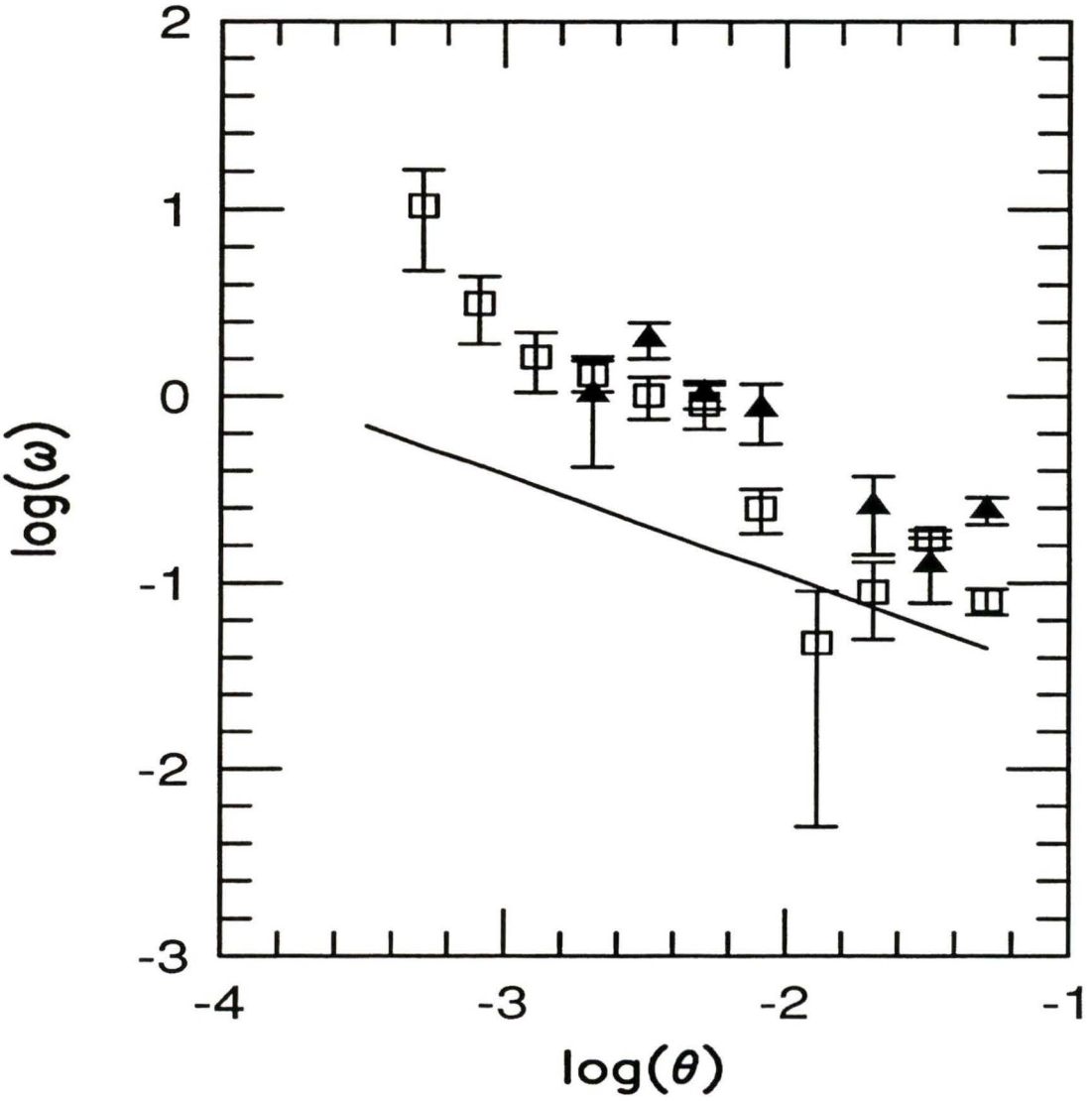

Figure 4.12: The Cross-Correlation function ω of bright ($19.5 < \left(\frac{J+F}{2}\right) < 20.5$) galaxies with the entire sample (open squares). Also shown is the autocorrelation of the bright sample (filled triangles). The solid line represents a fit to the Infante and Pritchet (1995) correlation function for their merged catalogue with amplitude and slope $A_\omega^{\delta=0.54}(1') = 0.083$ and covering the magnitude range $20 < \left(\frac{J+F}{2}\right) < 23$.

Chapter 5

Interpretation of Results

The results from the previous Chapter indicate that

- There is no excess over a power law fit in the correlation function at small separations.
- Galaxy pairs are slightly redder than the field galaxy population.
- Higher correlation amplitudes are observed for redder galaxies than bluer galaxies.

We will deal with each of these results in turn.

5.1 Correlation Function Excesses

At least one source in the literature (Carlberg et al., 1994) has reported an excess in the correlation function (that is, an excess over an inward extrapolation of $\omega(\theta)$) at the separations we investigate. Consequently it extremely important that the reduction process used to obtain the current correlation functions is carefully examined. The most obvious place where errors could

be made is the editing process (the catalogue editing process is described fully in Section 3.4). For example, in the J band catalogue, if editing is *not* performed, we find that $N_p(6'' - 24'')/N_p(3'' - 6'') = 9.6$, compared to the value produced by extrapolating the Pritchet and Infante correlation function of 16.7 and the observed value, *after* editing, of 17.1 ± 1.7 . Without editing, the correlation function appears to be in excess of the predicted value by almost a factor of two.

Furthermore, for the inner bin, before editing, $N_p(6''-24'')/N_p(1''-6'') = 4.62$, whilst after editing, the extrapolated and observed values are 12.2 and 11.8 ± 0.57 respectively, giving an excess *before editing* of approximately $\times 3$; it is apparent that inclusion of the discarded population has a dramatic effect on the pair counts. (Note that in Carlberg et al., they find a pair excess of $3 - 5\times$ for their V band samples.)

What fraction of the discarded population would need to be included in our pair sample to produce a measurable excess in the number of close pairs? From the discussion above we see that for the $3'' - 6''$ range the inclusion of the *entire* discarded population produces only a factor of two excess in the correlation function. To produce this excess for the $1'' - 6''$ sample requires the inclusion of an extra ~ 400 paired objects in the catalogues.

All discarded objects were carefully examined to ensure that they were not misclassified. It was found that, at most, only perhaps $5\% - 10\%$ of the catalogue objects might be real objects mistakenly discarded (the vast majority of discarded objects are obviously spurious objects such as multiple detections on large galaxies or stellar images). Inclusion of all these marginal detections, even if all of them contributed to the small separation pairs counts

(which they do not), amounts to an extra ~ 60 objects. This is not enough to produce the excess in pair counts observed in Carlberg et al. .

One other possibility is that systematic photometric errors are responsible for our null result. Carlberg et al. find that their correlation function excesses are smaller for fainter magnitudes. If all our magnitudes were systematically fainter, then this might reduce the observed correlation function amplitudes. However, our photometric calibrations have an error of at most only 0.2 mag by $J \sim 23$, not enough to lower the correlation amplitudes significantly (a 1-2 mag difference would be required). Furthermore, the present correlation functions agrees very well with those published (Infante and Pritchet, 1995); photometric errors of the amount required to produce the effect outlined above would result in correlation functions much lower than those found in Pritchet and Infante.

5.2 Pair/Field Colours

The lack of large colour difference between pair and field samples has been reported before in the literature (Carlberg et al., 1994; Zepf and Koo, 1989) and consequently our result is not surprising. To explain how merging events could occur and not affect pair colours, several arguments have been advanced: firstly, a large fraction of the *field* population has recently ($\sim 1-2$ Gyr) undergone merging and as a consequence no colour difference exists between pairs and field colours; secondly, the colour difference induced by merger events is below detectable limits; or, lastly, objects in the small separation bins are contaminated by a population of objects which are not physi-

cally associated but appear together only through projection effects–or, even if they are physically associated may not merge (perhaps as a consequence of large velocity differences). From the definition of the correlation function– the fractional number of objects in excess of a random distribution– we may estimate the number of physical pairs for any given $\omega(\theta)$. For example, when $\omega(\theta) \sim 1$ this means that the fraction of physical pairs in the sample is $\omega(\theta)/(\omega(\theta)+1) = 50\%$, whilst the remainder are projected pairs. For our sample, $\omega(1'' - 6'') \sim 0.54 \pm 0.2$ which implies that only 35% of our pairs are physical–the rest are projected.

A simple calculation can be performed to estimate how many mergers would have to occur in our sample before the colour difference between the merging and field populations would be detectable. A recent paper (Cole et al., 1994a) indicates that a instantaneous burst of star formation produces a change in $(B-V)$ colour of 0.3 over 3-4 Gyr. We may safely assume that $(B-V) \sim -(J-F)$ (Kron, 1980). Consequently, for our inner sample of 166 objects with colour information, we find that to produce a 1σ detection of this merging process would require that around $10\% - 20\%$ of the galaxy population participate in it. Of course, for our sample with its low correlation amplitude and consequent high contamination by non-physical pairs, this fraction would be much higher. Furthermore, we have reason to suspect that our merged catalogue is incomplete. Note that in Table 4.1 the pair fraction for the merged catalogue is *smaller* than that for the J or the F catalogue, indicating failures in object matching or photometry.

We conclude from the above that our sample is not sensitive to moderate amounts of merging in the galaxy population.

5.3 Red/Blue Correlation Amplitudes

The difference in correlation amplitudes found for the reddest 25% and the bluest 25% of galaxies in our sample is shown in Figures 4.5 and 4.6. These plots show that the correlation amplitude is significantly higher for the redder samples than for the bluer samples.

Furthermore, it is interesting to note that all samples in Table 4.2 indicate that objects in the inner bin are slightly *redder* than in the outer bin, in accordance with the slightly steeper slopes found for the redder sample.

We may explain the increased correlation amplitude found for redder galaxies by noting that this population is comprised predominately of late-type (i.e., older) galaxies which have *higher* intrinsic luminosity. It is known that elliptical galaxies have higher correlation amplitudes than other morphological types; for example, in the Center for Astrophysics Redshift Survey, it is found (Boerner and Mo, 1990) that elliptical and lenticular galaxies have a correlation strength of about 1.7 times that of spirals and irregulars.

5.4 Merger Rates

Galaxies are thought to have undergone more mergers in the past than at the current epoch. The merger rate is usually parametrised by an equation of the form $(1+z)^n$; to calculate the merger rate we must solve

$$\frac{(1+z_l)^n}{(1+z_f)^n} = \frac{f^l_{mg}}{f^f_{mg}} \tag{5.1}$$

for n, where z_l and z_f is the median redshifts of the local and faint galaxy

samples, respectively, whilst f^l_{mg} and f^f_{mg} are the fraction of galaxies in pairs at these two redshifts. For our local sample of galaxies, we use the UGC (Uppsala Galaxy Catalogue). The median redshift of the UGC sample, $z_l =$ is 0.007 whilst the median redshift of our sample is assumed to be the same as the measured median redshift of the Carlberg et al. sample, i.e., 0.4. This is reasonable as the magnitude limit of our sample is roughly the same as Carlberg et al.'s. Carlberg et al. find that for the UGC catalogue, the fraction likely to merge, $f_{mg} = 2.3 \pm 0.2\%$.

We wish to calculate f_{mg} for our faint sample. The number of galaxies separated by less than $6''$ for our J band catalogue is 528, corresponding to a pair fraction of $8.5 \pm 0.3\%$ (as already discussed in Section 4.2). We choose the value of $6''$ following dynamical considerations outlined in Carlberg et al.: at the redshift of our sample, galaxies separated by this amount or less can be considered as "doomed to merge". However, this pair fraction is contaminated by *projected* pairs. To find the number of physical pairs we must use the value of the angular correlation function at this separation. As described in Section 5.2, $\omega(1'' - 6'') = 0.54 \pm 0.2$ This corresponds to a physical pair fraction of 0.35 ± 0.07, which gives a faint physical pair fraction of $3.0 \pm 0.6\%$. Solving Equation 5.1 for n we get $n = 0.8 \pm 0.6$. This result is considerably different from that found by Carlberg et al., who find that $n = 3.1 \pm 1.0$. Our lower value of n is a direct consequence of the lower value of the correlation function used which results in a much smaller physical pair fraction at $z = 0.4$ than that used in Carlberg et al. .

5.5 Luminosity Evolution or Number Evolution?

Our intention in this work was to investigate how the galaxy population at intermediate redshifts evolves to the present-day population. We have attempted to accomplish this by investigating clustering and colour properties of galaxies separated by small ($\theta < 6''$) separations. This "faint blue galaxy problem", discussed in the introduction, may be summarised as follows: the distribution of galaxies in redshift space is well described by models in which galaxy properties do not change with time (the "no-evolution" models). However, observed number counts at faint ($J < 20$) magnitudes are much higher than the predictions of these models. Studies indicate that this excess population is *weakly clustered* and *blue* in colour.

The many theories that have been advanced to explain the nature of this excess population fall into three main groups.

- The *local* galaxy luminosity function is incorrect. Errors in the local luminosity function are postulated to arise from either incompleteness in the bright (i.e., $17 < J < 20$) counts or a large population of Low Surface Brightness (LSB) galaxies which are missed in current surveys because their surface brightness is below the limit of detectability. The very small number of galaxies with $17 < J < 20$, even in the largest surveys, means that these counts are very prone to statistical fluctuations. As many workers have pointed out, a factor of 2 difference in the local counts removes the excess in the faint blue counts. For example, Koo and Kron (Koo and Kron, 1992) claim to have derived a

luminosity function which fits both high and low redshift ends of the distribution, but the match between their local luminosity function and the observations is doubtful for at least one bandpass. Note that this explanation does not require any evolution in the galaxy luminosity function.

- The galaxy population undergoes merging. The merger event, in the classical picture (Larson and Tinsley, 1978), produces a burst of star formation. This burst increases the galaxy luminosity and causes the galaxy population to become *bluer*. The excess in the number counts is interpreted as brightening of more distant (more numerous) galaxies. Many different merging scenarios have been proposed. Merging scenarios (such as (Broadhurst et al., 1992) predict a difference between pair and field galaxy colours and an excess in the correlation function at small separations.

- The *faint end* of the local luminosity function is ill-defined. In these models, the count excess is interpreted as a large population of "bursting dwarfs" i.e., dwarf galaxies that are undergoing their first episode of star-formation, triggered by supernovae-driven winds. Dwarf galaxies in high-density environments survive this star-formation, whilst those those that are not are destroyed (Babul and Rees, 1992). Alternatively, the dwarf galaxies could still exist today but would not be visible in local catalogues because their surface brightness is below the limit of these catalogues. In addition, these models help to explain the lower correlation amplitude of faint galaxies as local surveys indi-

cate that dwarf/irregular galaxies have shorter correlation lengths than other morphological types.

Of course, the actual explanation of the problem may well be a combination of these three models. Furthermore, the data presented in the current work is not extensive enough (consisting only of magnitudes in two bandpasses for each galaxy, with no redshift information available) to distinguish between the many variants of the above models presented in the literature. However, we may still attempt to make broad comparisons between our data and these three models.

Given the large number of projected pairs in our sample, the colour information presented here is not to be considered reliable enough to detect whether merging or other interaction processes are producing *bluer* galaxy colours. In fact, our sample shows that the inner bins are slightly *redder* than the outer bins, a result explained above.

The similarity between pair and field objects and the lack of observed excesses in the correlation function force us to conclude that if merging *does* occur, it is below the level at which we are able to detect it.

Chapter 6

Summary

We may summarise this thesis as follows.

The production of three new galaxy catalogues was described. Two catalogues contain objects in the magnitude range $20 < J < 23$ and $19 < F < 22$, whilst a matched catalogue contains $J - F$ colours for all objects in the range $19.5 < \left(\frac{J+F}{2}\right) < 22.5$.

The editing process used to produce the catalogues was reviewed to determine if errors in object detection and classification could significantly affect the results. At most, approximately 10% of small separation catalogue objects are of uncertain nature. This error is not large enough to measurably affect the results.

Properties (primarily colour and clustering) of galaxies at small ($\theta < 6''$) angular separations were investigated, and the following conclusions were drawn:

Firstly, field galaxies are slightly redder (at the 1σ level) than paired galaxies. Furthermore, the correlation amplitude of redder galaxies is found to be higher than that of bluer galaxies. These results are interpreted as a

consequence of the higher correlation strength of later-type galaxies.

Secondly, the angular correlation function at small separations is well described by extrapolation of the (large angle) Pritchet and Infante correlation functions to these separations. In addition, ratios of pair counts in two angular bins ($1'' - 6''$ and $6'' - 24''$) agree well with predictions of the Pritchet and Infante correlation functions. Taken together, these two results argue there is no excess in close pairs of galaxies. This result is found for all three catalogues.

The low amplitude found for the correlation function in this work argues that the fraction of galaxies in *physical* pairs at small separations is small. Consequently, this implies that detection of merging by colour differences is quite difficult and would require a much larger number of galaxies than available in the current work. Furthermore, the low merger rates derived for our sample argue against significant merging in the galaxy population as described by Broadhurst et al (1988). Consequently, models in which the faint blue excess is explained in terms of starbursting dwarf galaxies or an incorrectly determined local luminosity function are favoured.

6.1 Future Work

The photographic data described in this thesis is of much lower quality (in terms of resolution and dynamic response) than is possible with modern Charge-Coupled-Devices (CCDs). Traditionally, photographic plates were preferred to CCDs for survey work by virtue of their large angular coverage. Recently, however, large format CCD detectors have become available, and

as a consequence it is now feasible to survey large parts of the sky with CCDs (large angular coverage is necessary because the density of close pairs on the sky is very low). Such a survey would not only provide accurate colour and clustering information for faint close pairs, but would also permit an investigation of the *morphologies* of close pairs. Direct evidence for large numbers of distorted or tidally disturbed paired galaxies would provide powerful support for merger models. Such surveys are now currently underway.

Imaging in different wavebands can also provide important insights into the faint blue galaxy problem. In the past few years near-infrared (known as the K band, $2.3\mu m$) detectors have been developed and are being used to survey the sky and produce number counts. The K light is relatively insensitive to star-formation in the galaxy populations and is therefore thought to accurately trace the evolution of galactic mass at distant (i.e., $z \sim 0.4$) epochs. Therefore, measurement of K band number counts at cosmologically significant redshifts provides valuable information concerning galaxy formation and merging. Furthermore, the K-band light corresponds to the rest-frame optical at $z \sim 0.4$; consequently corrections which must be applied to the number counts are much better understood than for the B band, where the present-day B light traces the far ultra-violet.

In addition to the imaging work outlined above, spectroscopic surveys are currently in progress which will provide redshifts for large numbers of paired galaxies. Carlberg et al. measured redshifts for paired and field galaxies, and found no statistically significant difference between them; however, their spectroscopic sample was very small and consequently subject to statistical fluctuations in their data. Existence of a significantly different redshift

for pair and field galaxies would argue strongly in favour of galaxy merger models.

Bibliography

Babul, A. and Rees, M. J.: 1992, *Mon. Not. R. Astron. Soc.* **255**, 364

Bernstein, G., Tyson, J., and Jarvis, J.: 1994, *Astrophys. J.* **426**, 516

Boerner, M. and Mo, H.: 1990, *Astron. Astrophys.* **227**, 324

Brainerd, T. G., Smail, I., and Mould, J.: 1994, *Mon. Not. R. Astron. Soc.* **244**, 408

Broadhurst, T., Ellis, R., and Shanks., T.: 1988, *Mon. Not. R. Astron. Soc.* **235**, 827

Broadhurst, T. J., Ellis, R. S., and Glazebrook, K.: 1992, *Nature* **355**, 55

Bunclarke, P. and Irwin, M.: 1992, SPIE

Carlberg, R., Pritchet, C., and Infante, L.: 1994, *Astrophys. J.* **435**, 540

Cole, S., Aragon-Salamanca, A., Frenk, C., Navarro, J. F., and Zepf, S.: 1994a, *Mon. Not. R. Astron. Soc.* **271**, 781

Cole, S., Ellis, R., Broadhurst, T., and Colless, M.: 1994b, *Mon. Not. R. Astron. Soc.* **267**, 541

Colless, M. M., Ellis, R. S., Broadhurst, T. J., and Peterson, B. A.: 1993, *Mon. Not. R. Astron. Soc.* **244**, 408

Colless, M. M., Ellis, R. S., Taylor, K., and Hook, R. N.: 1990, *Mon. Not. R. Astron. Soc.* **244**, 408

Cowie, L., Songaila, A., and Hu, E.: 1994, preprint

Groth, E. J. and Peebles, P.: 1977, *Astrophys. J.* **217**, 385

Infante, L.: 1987, *Astron. Astrophys.* **183**, 177

Infante, L. and Pritchet, C.: 1995, *Astrophys. J.* **439**, 565

Koo, D. C. and Kron, R. G.: 1992, *Annual Review of Astronomy and Astrophysics* **30**, 613

Koo, D. C. and Szalay, A. S.: 1984, *Astrophys. J.* **282**, 390

Kron, R.: 1980, *Astrophys. J., Suppl. Ser.* **43**, 305

Larson, R. and Tinsley, B.: 1978, *Astrophys. J.* **219**, 46

Peterson, B. A., Kibblewhite, R., and Brigeland, M.: 1979, *Astrophys. J.* **233**, L109

Press, W. H., Flannery, B. P., Teukolsky, S. A., and Vetterling, W. T.: 1986, *Numerical Recipes*, Cambridge University Press

Pritchet, C. and Infante, L.: 1992a, *Astrophys. J., Lett.* **399**, L35

Pritchet, C. and Infante, L.: 1992b, *Astrophys. J., Suppl. Ser.* **83**, 234

Roche, N., Shanks, T., Metcalfe, N., and Fong, R.: 1993, *Mon. Not. R. Astron. Soc.* **263**, 360

Seldner, M., Siebers, B., Groth, E. J., and Peebles, P. J. E.: 1977, *Astron. J.* **82**, 249

Shane, C. and Wirtanen, C.: 1967, *Publications of the Lick Observatory* **XXII**, Pt. 1

Shanks, T., Fong, R., and Ellis, R.: 1980, *Mon. Not. R. Astron. Soc.* **192**, 209

Tyson, J. A. and Jarvis, J. F.: 1979, *Astrophys. J., Lett.* **230**, L153

Zepf, S. E. and Koo, D. C.: 1989, *Astrophys. J.* **337**, 34

VITA

Surname: McCracken Given Names: Henry Joy

Educational Institutions Attended:

University of Victoria	1992 – 1995
University of Manchester Inst. Sci. & Tech.	1988 – 1991

Degrees Awarded:

B.Sc. (Honours)	University of Manchester	1991

Honours and Awards:

Graduate Teaching Fellowship	1992 – 1995

Partial Copyright Licence

I hereby grant the right to lend my dissertation to users of the University of Victoria Library, and to make single copies only for such users or in response to a request from the Library of any other university, or similar institution, on its behalf or for one of its users. I further agree that permission for extensive copying of this dissertation for scholarly purpose may be granted by me or a member of the University designated by me. It is understood that copying or publication of this dissertation for for financial gain shall not be allowed without my written permission.

Title of Dissertation:

Properties of Close Pairs of Galaxies

Author:

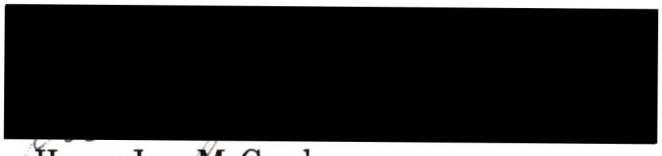

Henry Joy McCracken
April 27, 1995